eLife

Reviewed Preprint
v2 • September 26, 2024
Revised by authors

Reviewed Preprint
v1 • January 25, 2024

Cell Biology

Exceptional longevity of mammalian ovarian and oocyte macromolecules throughout the reproductive lifespan

Ewa K Bomba-Warczak, Karen M Velez, Luhan T Zhou, Christelle Guillermier, Seby Edassery, Matthew L Steinhauser, Jeffrey N Savas, Francesca E Duncan

Department of Neurology, Northwestern University Feinberg School of Medicine, Chicago, United States • Department of Obstetrics and Gynecology, Feinberg School of Medicine, Northwestern University, Chicago, United States • Department of Medicine, Division of Genetics, Brigham and Women's Hospital, Boston, United States

Abstract

The mechanisms contributing to age-related deterioration of the female reproductive system are complex, however aberrant protein homeostasis is a major contributor. We elucidated exceptionally stable proteins, structures, and macromolecules that persist in mammalian ovaries and gametes across the reproductive lifespan. Ovaries exhibit localized structural and cell-type specific enrichment of stable macromolecules in both the follicular and extrafollicular environments. Moreover, ovaries and oocytes both harbor a panel of exceptionally long-lived proteins, including cytoskeletal, mitochondrial, and oocyte-derived proteins. The exceptional persistence of these long-lived molecules suggest a critical role in lifelong maintenance and age-dependent deterioration of reproductive tissues.

One sentence summary

Exceptionally long-lived macromolecules in mammalian ovaries and oocytes as pillars for lifelong reproductive health span.

eLife assessment

This **important** study highlights cell types preserving long-lived proteins and lays a foundation for identifying exceptionally long-lived proteins in the ovary. **Convincing** evidence describes helpful data about protein turnover and identifies long-lived macromolecules in oocytes and somatic cells during mouse ovarian aging. This work will be of interest to researchers working on aging and reproductive health.

https://doi.org/10.7554/eLife.93172.2.sa4

Main Text

The female reproductive system is the first to age in the human body with fertility decreasing for women in their mid-thirties and reproductive function ceasing completely at menopause (1). In the ovary, aging is associated with a loss in gamete quantity and quality which contributes to infertility, miscarriages, and birth defects (2-5). Moreover, the age-dependent loss of the ovarian hormone, estrogen, has adverse general health outcomes (6). These sequelae are significant as women globally are delaying childbearing and the gap between menopause and lifespan is widening due to medical interventions (7, 8). Although aging is a multifaceted process, loss of proteostasis and dysfunctional protein quality control pathways are hallmarks of reproductive aging (9).

Proteostasis relies on tight inter-regulation of protein synthesis, post-translational modifications, folding, and degradation (10). While most protein lifetimes in mammals fall within the scale from hours to days (11, 12), a subset of intracellular proteins persists for months in rodents (13, 14). These long-lived proteins (LLPs) are enriched in tissues harboring long-lived post-mitotic terminally differentiated cells, such as the brain and heart (13-15). Although the extended lifespan of LLPs places them at inherent risk for accumulating damage during aging, many of them provide key structural support for the lifelong maintenance of highly stable protein complexes in cells (16).

The mammalian ovary is comprised of a fixed and nonrenewable pool of long-lived cells or oocytes. In humans, oocytes initiate meiosis during fetal development, and by birth, all oocytes are arrested at prophase of meiosis I (17, 18). This cell cycle arrest is maintained until ovulation, which occurs any time between puberty and menopause, and thus can span decades. The oocytes are particularly sensitive to protein metabolism alterations because they contribute the bulk cytoplasm to the embryo following fertilization. Thus, maternal proteins produced during oogenesis are essential to generate high-quality gametes (9). The ovarian microenvironment is a critical determinant of gamete quality and has been shown to become fibro-inflamed and stiff with age (19-21). Although a small number of oocyte-specific proteins have been identified as long-lived, including cohesins and several centromere-specific histones, there has not been a discovery-based approach to define the long-lived proteome of the ovary and oocyte. Thus, the potential contribution of LLPs to the age-related deterioration of the reproductive system in mammals remains to be elucidated. In this study we used multi-generational whole animal metabolic stable isotope labeling and leading mass spectrometry (MS)-based quantitative proteomic approaches to visualize and identify ovarian and oocyte long lived macromolecules in *vivo* during milestones relevant to the reproductive system.

Exceptional longevity of ovarian structures and molecules in mammals

The mammalian ovary is a structurally complex, heterogenous, and dynamic organ with follicles at different stages of development, remnants of ovulation (corpora lutea), and a heterogeneous stroma (22) (**Fig. 1A**). Very little is known about the long-term homeostasis and relative turnover of the ovarian tissue components during aging. To address this, we visualized the lifespan of ovarian macromolecules in mammals using a combination of stable isotope labelling and multi-isotope imaging mass spectrometry (MIMS) (**fig. S1A**). First, using a two-generational metabolic labelling of animals with ^{15}N, we generated a cohort of fully ^{15}N-labelled pups. After birth, labelled females were kept with the labelled dam until weaning, at which time their food source was switched to the ^{14}N-chow chase. Using previously established methods (9, 23-25), we determined that chase periods of 6 and 10 months represented a biologically relevant reproductive aging continuum as mice within this age range begin to manifest ovarian

aging phenotypes, including follicle loss (**fig. S1B-D**), decreased ovulation (**fig. S1 E and F**), and increased fibrotic foci in the ovarian stroma (**fig. S1 G-J**). Importantly, sufficient numbers of oocytes can still be collected at these timepoints for meaningful further downstream analyses of this rare cell type. We first performed MIMS on ovarian sections to visualize and quantify the abundance of ^{14}N, representing molecules which have been replaced during the chase period (blue-teal), and ^{15}N, which represents ^{15}N-containing molecules that must have persisted through the chase period and therefore are long-lived (orange-pink) (**Figs. 1B**, **S2 A and B**) (26-28). Within the ovarian follicles, MIMS revealed a strikingly higher abundance of ^{15}N containing molecules in primordial and primary stages relative to later stage follicles, suggesting that primordial follicles can persist for months with limited macromolecular turnover (**Fig. 1C**). As follicles progress through the primary, secondary, and antral stages the $^{15}N/^{14}N$ ratio decreases due to signal dilution associated with the increase of cell number and follicle growth (**Figs. 1C**, **S2 C**). This change in ^{15}N abundance was most apparent in the granulosa cells where long-lived molecules were significantly higher in those within primordial and primary follicles compared to later follicle stages (**Fig. 1C** and **F**). In addition to granulosa cells, long-lived molecules also localized to the basement membrane of some early growing follicles (**fig. S1D**). Beyond the follicle, other somatic compartments of the ovary were additionally found to have higher ^{15}N:^{14}N ratio suggesting enrichment in long-lived components, including steroidogenic cells (theca layer and corpora lutea), stromal cells, and cells within the ovarian surface epithelium (OSE) (**Fig. 1 B and D**). Our quantitative analysis revealed that the OSE had significantly higher $^{15}N/^{14}N$ ratio among the mentioned cell types (**Fig. 1G**). Lastly, we analyzed the $^{15}N/^{14}N$ ratios in the nucleus relative to the cytoplasm, which revealed significant enrichment of long-lived, ^{15}N-positive molecules in the nuclei of granulosa cells within primary follicles, and cells within the corpora lutea, the stroma, and the OSE. (**Fig. 1E and H**). As both proteins and nucleic acids contain nitrogen, the ^{15}N-positive nuclear signal could correspond to known long-lived nuclear proteins, such as histones, nuclear pore proteins, and lamins, which were previously identified in neuronal, post-mitotic cells (14, 15). Alternatively, as these nuclear ^{15}N-hotspots coincided with the ^{31}P signal, which is enriched in DNA and correlates with DNA labeling(29), this data may suggest that the DNA itself is long-lived (**Fig. 1E**). These results reveal that distinct macromolecular components within select ovarian cells and tissue regions persist throughout the healthy reproductive stage, with limited renewal, and those long-lived molecules persist through the stage where ovaries manifest marked reproductive aging phenotypes.

Identification of the long-lived proteome in mammalian ovaries

Although MIMS analysis provides important spatial information on long-lived structures in the ovary, it does not provide the identity of ^{15}N-containing macromolecules that comprise them. To address this, we performed liquid chromatography mass spectrometry (LC-MS/MS)-based proteomic analysis of ovarian tissues isolated from metabolically labeled mice. After 6-months of ^{14}N-chase, we identified 36,222 ± 6768 ^{14}N-peptides mapping to 4106 proteins, and 13 ± 5 ^{15}N peptides, which collectively mapped to 33 LLPs across all the biological replicates (**Fig. 2 A and B**, table S1). To gain a deeper insight into the persistence of LLPs beyond 6 months, we also analyzed ovaries isolated from females that remained on ^{14}N chase for 10 months. Although the total numbers of both ^{14}N and ^{15}N peptides and proteins were similar between the two timepoints (39,637 ± 12005 ^{14}N-peptides mapping to 4464 proteins and 13 ± 6 ^{15}N peptides mapping to 15 LLPs), the majority of LLPs identified at 6 months were no longer identified as long-lived at the 10-month chase timepoint. Only tubulins and select histones persisted and were identified as LLPs at this aged timepoint. Gene ontology (GO) enrichment analysis of LLPs identified at the 6-month chase timepoint revealed significant overrepresentation for terms related to chromatin, nucleosome, tubulin complex, and mitochondria (**Fig. 2C**).

Next, we determined the quantity of each LLP remaining after the ^{14}N-chase period by calculating the fractional abundance (FA; ^{15}N remaining, $^{15}N/[^{14}N + ^{15}N]$) for each LLP in the ovary using reconstructed MS1 chromatograms from LC-MS/MS analysis (30) (**Fig. 2 D-F**). We found that

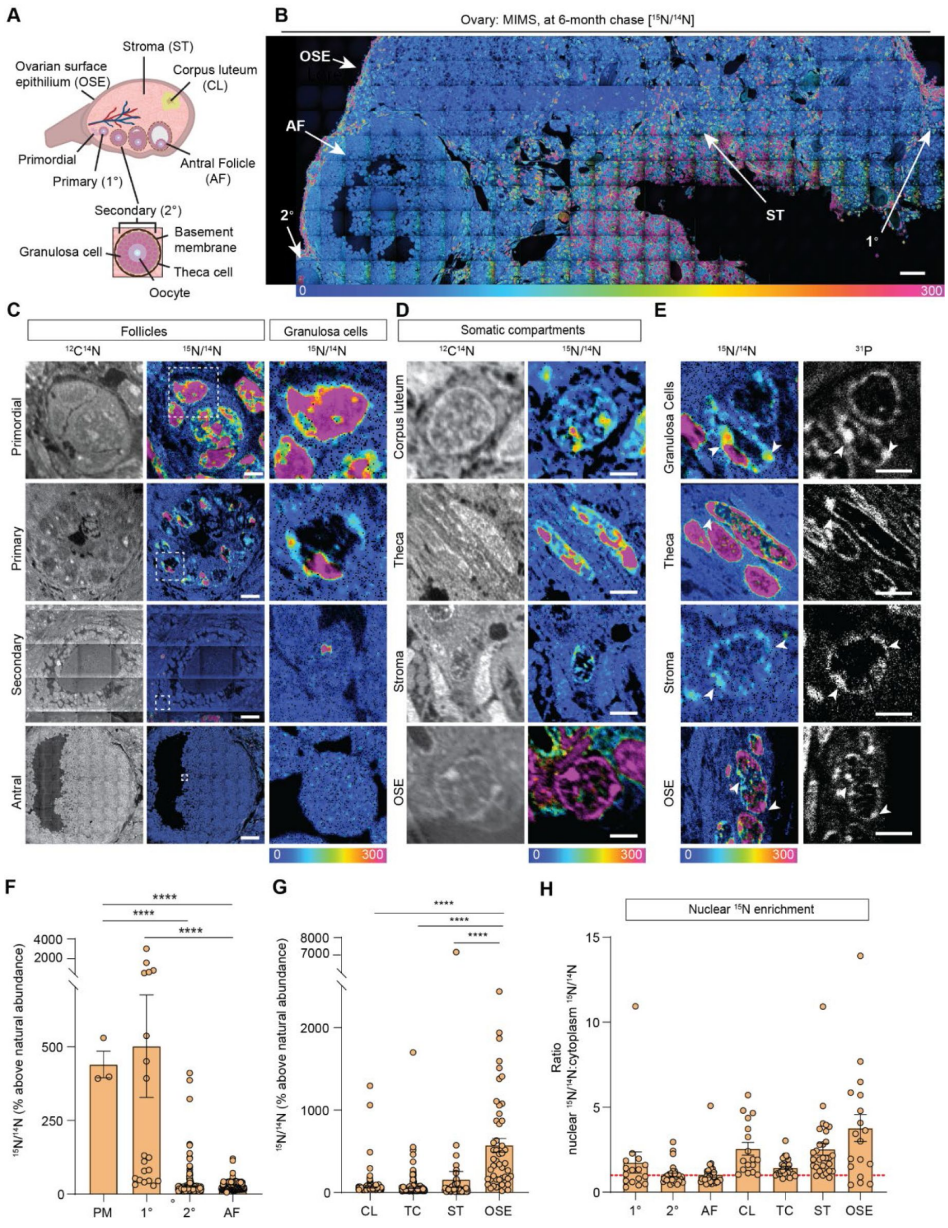

Fig. 1

MIMS analysis of cells and structures across ovarian tissue sections.

(A) Diagram depicting and defining structures of the mammalian ovary. **(B)** Representative hue saturation intensity (HSI) mosaic from an ovary of a ^{15}N labeled mouse (6 months old). Localization and abundance of ^{15}N varied depending on cell type. HSI scale was set to 0% (natural $^{15}N/^{14}N$ ratio) to 300% (above the natural ratio). Scale bar = 60 μm. **(C)** High abundance of ^{15}N is seen in early-stage follicles, specifically within granulosa cells. **(D)** Representative images of somatic cells show differences in ^{15}N labeling. **(E)** Intracellular abundance of ^{15}N is colocalized with ^{31}P abundance across all cell types. **(F)** Differences in $^{15}N/^{14}N$ ratios reveal granulosa cells of early-stage follicles have greater ^{15}N abundance than later stages. **(G)** Among somatic cells, quantitative analysis shows a greater abundance of ^{15}N at the ovarian surface epithelium. **(H)** Ratio analysis show abundance of ^{15}N localized in nuclear regions of cells. A hypothetical ratio of one, denoted as a red dash line, signifies no difference in ^{15}N abundance between cytoplasmic and nuclear regions. Abbreviations: PM (primordial follicle), 1° (primary follicle), 2° (secondary follicle), AF (antral follicle), CL (corpus luteum), TC (theca cell), ST (stroma), and OSE (ovarian surface epithelium). HSI scale for all images was set to 0%-300% (above natural abundance). Data are shown as mean±SEM. Statistical analysis was performed using a one-way ANOVA. Asterisk denotes statistical significance (* p≤.05; ** p≤.01; *** p≤.001; **** p≤.0001). Scale bar = (B): 50 μm; (C): 3 μm (PR), 6 μm (1°), 30 μm (2°), 75 μm (AF); (D): 2.5 μm (CL), 2.5 μm (TC), 5 μm (ST), 2.5 μm (OSE); (E): 3 μm (GC), 3 μm (TC), 2.5 μm (ST), 6 μm (OSE).

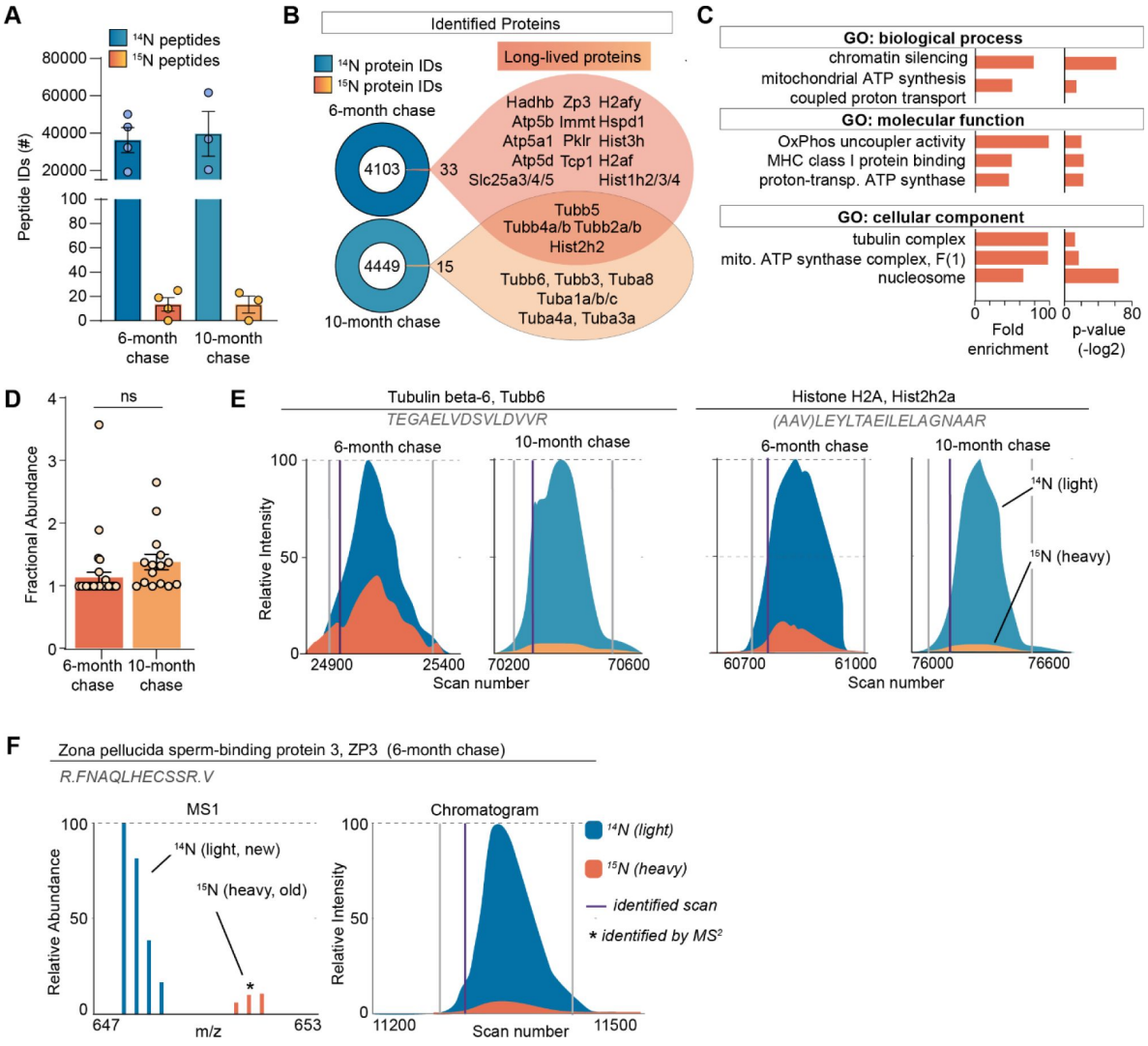

Fig. 2.

Long-lived proteome in mammalian ovaries.

(A) Summary of peptide identification at 6 and 10-month chase points, blue graphs indicate ^{14}N peptide IDs, orange/yellow graphs indicate ^{15}N peptide IDs. **(B)** Summary of protein identification at each time point, with a list of proteins identified as long-lived in orange. **(C)** GO analysis of the LLPs identified in ovaries at 6-months chase revealed that terms related to chromatin, nucleosome, tubulins, and mitochondria are significantly enriched. **(D)** Fractional abundance of LLPs identified at 6 and 10-month chase. **(E)** Annotated representative chromatograms of two representative proteins that persist through both 6- and 10-montch chase, illustrating the decreasing ^{15}N-signal over time. blue - 14N (new), orange 15N (old), purple line: identified scan. (**F)** Annotated representative raw MS1 scan of Zona Pellucida protein 3 (ZP3). Mean ± SEM; 3-4 biological replicate per timepoint, ns – not significant by Student's t-test.

LLPs had significant differences in FA between the 6- and 10-month time points, with 1.13 ± 0.08 % and 1.37 ± 0.12 % ^{15}N-remaining, respectively (**Fig. 2D**). The discrete pool of proteins that persisted throughout both time points allowed for a unique direct comparison of ^{15}N to ^{14}N-peptide peak intensities. This analysis showed reduced abundance of ^{15}N at the 10-month chase timepoint, consistent with continual, albeit slow, turnover of the protein pool (**Fig. 2E**). Interestingly, at the 6-month chase timepoint, we identified ^{15}N peptides mapping to an oocyte-specific protein, Zona pellucida-3 protein (ZP3), indicating that a pool persists without turnover for at least 6 months, but less than 10 months, as long-lived ZP3 was no longer identified at the 10-month timepoint (**Fig. 2F**). While histones and tubulin have been previously identified as LLPs in the mammalian brain and heart tissues, the 6-month long persistence of ZP3 in mouse ovaries is unexpected and of potential importance to reproductive biology.

Exceptional longevity of mitochondrial and myosin proteins in mammalian oocytes

MIMS analysis of ovarian sections also captured oocytes at various stages of development, which in addition to the enrichment of ^{15}N-signal within the oocyte nucleus, revealed multiple smaller cytoplasmic ^{15}N-hot spots (**Fig. 3A**). Thus, to determine the identity of these ^{15}N-enriched molecules we isolated fully grown oocytes from ovaries of labeled mice at 6 and 10 months chase timepoints followed by LC-MS/MS analysis (**Fig. 3B** and **S3A**). In oocytes, we identified a total of 2919 proteins at 6-months and 3234 proteins at 10-months (**Fig. 3B**, table S2). Although after 6-months of chase, we identified 146 LLPs in oocytes, only 11 LLPs were identified after 10-months, indicating that by this timepoint a vast majority of LLPs have been degraded and renewed. Interestingly, the GO analysis of LLPs in oocytes identified at 6-month timepoint revealed a significant enrichment of terms related to nucleosomes, myosin complex and several additional terms related to mitochondria including - OxPhos complexes, mitochondrial nucleoid, TCA cycle complexes, and mitochondrial permeability transition pore complex (**Fig. 3B**).

Next, we quantified the fraction of each protein pool that persisted for 6 or 10 months by calculating fractional abundance (FA) values, where the higher the value the longer-lived the corresponding proteins are (**fig. S3B**). Overall, there was no significant difference in FA between the two chase timepoints, with 41 ± 2.9 and 50.8 ± 12.2 ^{15}N-remaining at 6 and 10-months, respectively (**fig. S3C**). The higher average FA average at 10-month chase is likely due to turnover of proteins with lower FA values at 6 months, which by 10-months would leave the oocyte with the most persistent pool of proteins. In agreement, the FA values for 4 LLPs that were identified at both time points (Hba, Atp5a, Atp5B, and Hist1h4a) sharply decline between 6 and 10 months (**fig. S3D**), demonstrating protein degradation and replenishment. Considering the high abundance of mitochondrial proteins in our data set, and recent reports showing that expression of mitochondrial proteins is suppressed in aging oocytes (31), we compared the number of mitochondrial proteins and spectral counts identified (**fig. S3E and F**), as well as fractional abundance (**fig. S3G**) for mitochondrial proteins across the two timepoints. Our results indicate that while there are no significant differences in total mitochondrial protein abundance at 6- and 10-months post-chase, the pool of long lived mitochondrial proteins decreased significantly, with the majority of proteins being turned over at the later timepoint.

Hierarchical clustering of the LLPs identified at the 6-month timepoint revealed mitochondrial proteins and myosins as the two protein groups with the highest fractional abundance in the oocyte (**Fig. 3C**). In particular, mitochondria exhibited a wide range of FA values ranging from 1.10% to 98.9%, with an average of 55.9 ± 35.1 of ^{15}N-remaing at 6-months (table S2). FA values for myosins was markedly higher than both actin and tubulin with an average FA value of 80.97 ± 19.8 % for myosins, 31.4 ± 15.6% for actins, and only 8.3 ± 1.4% for tubulins. This indicates that while all three cytoskeletal components are long-lived, nearly 81% of the myosin protein pool persists throughout the 6-month timepoint, whereas only 31% of actin protein pool and 8.3% of tubulin protein pool persists throughout the same length of time. Histones were also identified as LLPs in

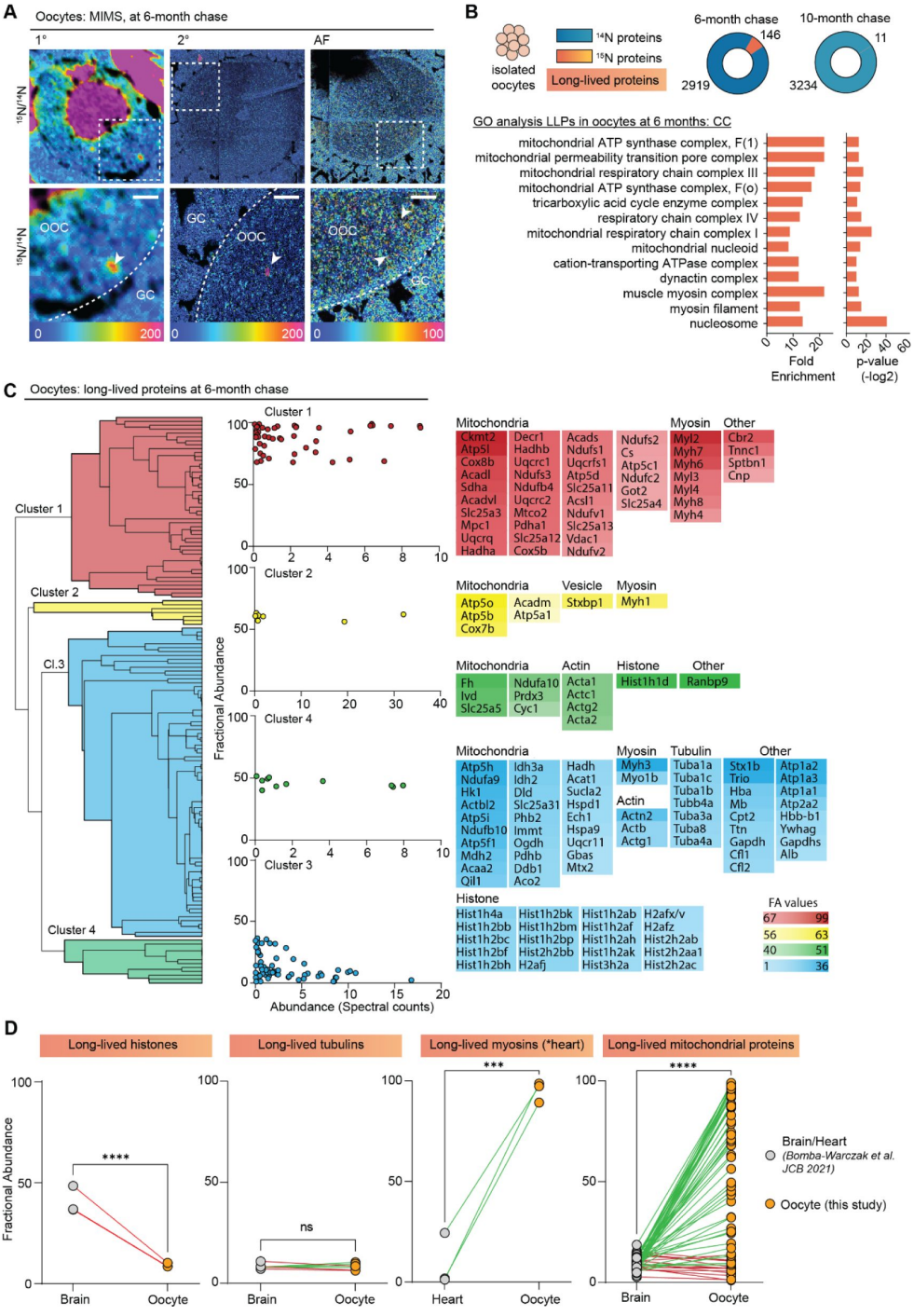

Fig 3.

Exceptional longevity of nuclear, cytoskeletal, and mitochondrial proteins in mouse oocytes.

(A) MIMS analysis reveals high abundance of ^{15}N in nuclei and throughout the cytoplasm of oocytes. **(B)** Purified oocyte population was harvested from pulse-chased mice and analyzed using gel-LC-MS/MS. Charts illustrate the number of proteins identified at each timepoint (blue) along with long-lived proteins (orange). GO analysis of the LLPs identified in oocytes at 6-months chase revealed an enrichment for terms related to nucleosome, myosins, and mitochondria. **(C)** Hierarchical cluster analysis of fractional abundance of LLPs identified in oocytes. **(D)** Direct comparison of fractional abundances of proteins previously identified as long-lived and LLPs in oocytes. Mean ± SEM; Oocytes collected from 4-7 females per time-point, *** p-value <.001, **** p-value < .0001 by Kruskal-Wallis ANOVA with Tukey's multiple comparisons test. Scale bar = 4 μm.

oocytes with average FA values of 7.7 ± 9.8. Mitochondrial proteins, histones, myosins, and tubulins have been previously identified as LLPs in brain and heart tissues, which are known to contain long-lived terminally differentiated cells (i.e. neurons in the brain and cardiac myocytes in the heart) (13). Importantly, however, this is the first time that a subset of the same proteins has been identified as long lived in the germ cell (**Fig. 3D**). Interestingly, the fractional abundance of mitochondrial LLPs in the brain (10.2 ± 6.6%)(13) and myosins in the heart (4.6 ± 8.1%)(13) is much lower in than the same LLPs quantified in the oocyte (55.9 ± 35.1)(**Fig. 3D**). In contrast, histones were less long-lived in the oocyte compared to the brain, and there was no significant difference observed for tubulins (**Fig. 3D**). Thus, although the identity of long-lived proteins may be conserved across tissues with long-lived cells, differences in fractional abundance may reflect tissue specific functions and requirements.

Discussion

In this study, multi-generational whole animal metabolic stable isotope labeling, paired with multi modal MS-based quantitative approaches enabled visualization and identification of ovarian and oocyte long lived macromolecules in vivo. Our findings provide a novel framework for how long-lived structures may regulate gamete quality. Long-lived macromolecules localized throughout the ovary including the follicular compartment with prominent signals in the granulosa cells of primordial and primary follicles relative to later stage growing follicles. These findings are consistent with the knowledge that the squamous pre-granulosa cells surrounding the oocyte within primordial follicles form early in development which coincided with the ^{15}N-labelling pulse period. These squamous granulosa cells are generally thought to lack the ability to undergo mitotic division until follicles are activated to grow, so it is not surprising that we observed long lived macromolecules persisting within them (32). In contrast, granulosa cells in growing follicles are generated by cell divisions that take place during follicle activation and growth which coincided with the ^{14}N-chase period. Thus, long-lived structures (i.e. enriched with ^{15}N) were diluted through cell divisions during follicle growth. Moreover, during follicle growth, granulosa cells proliferate and differentiate adding new pools of synthesized proteins and molecules. Our results demonstrate that macromolecules formed early in development can persist in squamous granulosa cells for months. Thus, it is possible that these long-lived molecules will accumulate more damage in primordial follicles that remain quiescent for longer periods relative to those that activate earlier. Whether such damage occurs and how it translates into decreased follicle survival or gamete quality will require further investigation.

Within the extrafollicular ovarian environment, the OSE exhibited a striking enrichment of long-lived molecules. The OSE is highly dynamic due to repeated post-ovulation wound healing and repair, and its regenerative capacity occurs through a somatic stem/progenitor cell-mediated process (33). Interestingly, long-lived proteins are retained in other cells undergoing repeated asymmetric divisions and are speculated to contribute to the reproductive aging process (34). Consistent with this possibility, the architecture and wound healing ability of the OSE is altered with advanced reproductive age (35). Furthermore, nuclear enrichment of the ^{15}N signal was highest in cells of the OSE. It is plausible that the older template DNA is segregated into the daughter cell destined to become the stem cell to ensure genetic stability of the OSE. Better understanding of the dynamics of long lived molecules in the OSE will require generation of specific samples at precise stages of the estrous cycle and across a time course of ovulation to capture follicular rupture and repair.

Through LC-MS/MS analysis, we identified specific long-lived proteins in the mammalian ovary across the reproductive lifespan. LLPs tend to be part of large protein complexes and include histones, nuclear pore complex proteins, lamins, myelin proteins, and mitochondrial proteins (16). In the ovary, the major categories of LLPs included histones, cytoskeletal proteins, and mitochondrial proteins. ZP3 was an oocyte-derived protein identified to be long-lived for at least 6

months. ZP3 is a protein that comprises the zona pellucida (ZP) or glycoprotein matrix of the oocyte, and it is expressed in oocytes of actively growing follicles beginning at the primary stage when the ZP begins to form (36). However, during the pulse period, there would have been very few growing follicles in the ovary because of the immature age of the mice, and most importantly, none of these follicles would have persisted 6 months since folliculogenesis only takes approximately 21 days (37). These findings suggest that ZP3 may be expressed earlier in oocyte development than previously anticipated. Because LLPs can be at the core of scaffold complexes, a primitive zona may exist at the primordial follicle stage upon which the bona fide ZP is established in growing follicles (38, 39). Consistent with this, expression of ZP proteins has been observed in human primordial follicles (39). Interestingly, there are documented age-related defects in the structure and function of the ZP which occur with time-dependent scaffold deterioration. An alternate explanation for our observation is that ZPs from atretic follicles persist and become incorporated into the ovarian matrix. Precedent for this exists because ZP proteins have been identified as components of the matrisome of decellularized porcine ovaries (40). Interestingly we did not identify ZP3 as an LLP in isolated fully grown oocytes which provides further support that in the ovary, the long-lived pool of ZP3 is derived from primordial follicles or are within the matrix. These possibilities require further investigation and may not be mutually exclusive.

Most LLPs were degraded and replaced between 6-10 months of chase. At the 6 month time point, we detected more long lived proteins than the 10 month time point in both the ovary and the oocyte because proteins degrade over time, and more time has elapsed at the later time point. Moreover, between the 6 and 10 month time points, age-related tissue dysfunction is already evident in the ovary. For example, in 6-9 month old mice, there is already a deterioration of chromosome cohesion in the egg which results in increased interkinetochore distances (41), and by 10 months, there are multinucleated giant cells present in the ovarian stroma which is consistent with chronic inflammation (20). Thus, our results suggest that important shifts in the proteome occur during mid to advanced reproductive and may be another early feature of ovarian aging. Whether the LLPs at the 6 month time point serve as a protective mechanism in maintaining gamete quality or whether they contribute to decreased quality associated with reproductive aging is an intriguing dichotomy which will require further investigation.

A small subset of tubulins and histones persisted throughout the entire 10-month chase period, indicating that their replacement is exceptionally slow. LLPs which were present at both time points and persisted to at least 10 months may have important roles in the aging process. Interestingly, Tubb5 and Tubb4a have high homology to primate-specific Tubb8, and Tubb8 mutations in women are associated with meiosis I arrest in oocytes and infertility (42, 43). Thus, perturbation of these particular proteins by virtue of their long-lived nature may be associated with impaired function and poor reproductive outcomes, and these possibilities warrant future investigation. We noted that LLPs identified at 10 months were not always identified as long-lived at 6 months. This is a common limitation of mass spectrometry-based proteomics where each sample is prepared and run individually, which introduces variability between biological replicates, especially with respect to low abundant proteins. To compensate for this known and inherent variability, we applied stringent filtering criteria where we required long-lived peptides to be identified in an independent MS scan which provided us peptides of highest confidence.

By isolating fully grown oocytes from the ovary, we were able to determine the long-lived proteome of a purified germ cell population across the reproductive lifespan. Although we identified certain histone proteins as long lived, their relative fractional abundance was much lower than in the brain, a tissue which also contains post-mitotic cells (14, 15). However, histone-variant exchange occurs continuously during mouse oogenesis and is required for both transcriptional regulation and de novo DNA methylation (44). Thus, turnover and exchange of histones is likely more dynamic than previously assumed in terminally differentiated or post-mitotic cells, and our findings are consistent with this in the oocyte. Myosin and actin were also

identified as LLPs with relatively high fractional abundance indicating exceptional longevity beyond 6-months. These proteins play numerous roles in oocyte maturation, fertilization, and egg activation, including nuclear positioning, spindle rotation and anchoring, chromosome segregation, cytokinesis, cortical granule exocytosis, and cytoplasmic flow (19, 45-49). Defects in many of these processes have been reported with advanced reproductive age, but whether long-lived pools of actin and myosins contribute to this etiology remains to be elucidated (50). Interestingly, F-actin stabilization restricts chromosome segregation errors due to cohesion loss which increase with age, so long lived pools of actin may confer a beneficial effect and protect against aneuploidy (49). The molecular mechanism(s) governing the longevity of the specific identified proteins in oocytes and ovaries as well as their relationship to the age-related decline in fertility and ovarian function require further investigation.

Mitochondrial proteins were the predominant LLPs in isolated oocytes across the reproductive lifespan, and it is plausible that ^{15}N cytoplasmic hotspots in oocytes that were observed in MIMS may correspond to mitochondria. Various aspects of mitochondrial dysfunction have been long-implicated in the age-dependent decline in gamete quality, with an age-dependent decrease in the number of mitochondria, an increase in abnormal morphology, and altered subcellular distribution (51). Moreover, mtDNA copy number decreases with age, whereas mtDNA mutations increase (52, 53). Finally, the functional capacity of mitochondria decreases with age with decreased membrane potential, increased reactive oxygen species, increased oxidative stress, and decrease energy output (54). Although it is possible that oocyte long lived mitochondrial proteins deteriorate with age and contribute to mitochondrial dysfunction, a different model is emerging for these proteins. Mitochondrial proteins are exceptionally long lived in tissues containing long-lived terminally differentiated cells and have now been documented in the brain (neurons), heart (cardiac myocytes), and the ovary (oocytes) (13). These mitochondrial LLPs are primarily localized to the cristae invaginations, which are throughout to serve as long-term stable ultrastructure within mitochondria. This strategic enrichment is hypothesized to serve as a lifelong structural pillar of mitochondria to support and maintain these organelles over long time frames (16). Although mitochondrial LLPs persist for at least 6 months in oocyte, the majority were undetectable by 10 months. Thus, it is tempting to speculate that a stable pool of mitochondrial LLPs provides structural support for the maintenance of mitochondrial structure and function early during the reproductive lifespan. However, turnover of mitochondrial LLPs later in the reproductive lifespan may serve as a biological timer of aging. Because mitochondria are maternally inherited, these mitochondrial LLPs formed during fetal development of the mother are likely transferred to the embryo and impact subsequent generations (55). Further investigation into the role of long-lived mitochondrial proteome in oocytes is necessary to understand their life-long contribution to reproductive health and fertility outcomes.

Additional information

Funding

This research was supported by NICHD R21HD098498 to JNS and FED, NIA R21AG072343 to JNS. EKBW was supported by the NINDS F32 NS106812 and NINDS K99NS126639.

Author contributions

Conceptualization: EKBW, JNS, FED; Methodology: JSN, FED, EKBW, KMV, LTZ, SE, CG, FG, MS, Investigation: EKBW, KMV, LTZ, SE; Visualization: EKBW, KMV; Funding acquisition: JNS, FED; Project administration: JNS, FED; Supervision: JNS, FED; Writing – original draft: EKBW, KMV, JNS, FED; Writing – review & editing: all authors.

Competing interests

The authors declare no competing interests.

Data and materials availability

All data generated or analyzed during this study are included in the manuscript and supporting files. RAW MS data has also been deposited at MassIVE under the accession number MSV000092217

Supplementary Materials

Materials and Methods

Animals

Mice of the FVB strain were obtained from Jackson Laboratory (Bar Harbor, ME). For the whole animal isotope pulse-chase labeling strategy, female (5 weeks old) and male mice (10 weeks old) mice were obtained. To validate the biological relevance of our chase period, reproductive aging parameters were evaluated in unlabeled female mice at 6 weeks, 6 months, and 10 months of age. Retired female FVB mouse breeders were obtained at 15 weeks of age and aged out to 6 months and 10 months. Mice were acclimated in the vivarium upon arrival for at least two weeks prior to experimental use. All mice were housed at Northwestern University's Center for Comparative Medicine under constant temperature, humidity, and light (14 hours light/10 hours dark). Mice were fed and provided with water *ad libitum*. All animal care and experimental protocols in this study were conducted under the guidelines set by the NIH Guide for the Care and Use of Laboratory Animals handbook, and the animal protocol was approved by the Animal Care and Use Committee of Northwestern University.

Pulse-chase labeling strategy

Mice were metabolically labeled using a two-generation metabolic pulse-chase labeling strategy as previously described (13). Briefly, three female FVB mice were fed a spirulina ^{15}N-containg chow for the duration of the study (initial labeling, breeding, pregnancy, and weaning) (Cambridge Isotope Laboratories, Inc., Tewksbury, MA). After 13 weeks of being on a ^{15}N diet, these labeled females were co-housed with unlabeled males for 5 days to allow a complete estrous cycle for breeding. Pregnant females were housed separately to allow for accurate dating of litter births. All females were allowed to breed a total of 3-5 times to obtain sufficient pups for the chase period. The pulse period was defined as the timespan between gestation and weaning of pups. Thus, pups conceived from labeled females had nitrogen-containing molecules and proteins labeled with ^{15}N. At 22 days old, pups were weaned and fed a ^{14}N diet *ad libitum*. Pups were maintained on a ^{14}N diet (chase) until they reached 7 and 11 months of age at which point tissues were harvested for downstream analyses. This animal labeling strategy generated 19 female pups. For ovary studies, 4 mice were used at 6 months post-chase and 4 mice at 10 months post-chase. One ovary per mouse was used for MIMS, and the contralateral ovary was used for LC-MS/MS. For oocyte studies, 4 mice were hyperstimulated at 6 months post-chase and 7 mice at 10 months post-chase. A total of 104 and 45 oocytes were collected at 6 months and 10 months post-chase, respectively, and these samples were used for LC-MS/MS.

Ovary and oocyte collection

Ovaries were harvested and placed in a dish containing pre-warmed Leibovitz's medium (L15) (Life Technologies Corporation, Grand Island, NY) supplemented with 3 mg/mL polyvinylpyrrolidone (PVP) (Sigma-Aldrich, St. Louis, MO), 0.5% penicillin-streptomycin (Life Technologies) (L15-PVP). Ovaries were either processed as described below for downstream analyses or used to isolate oocytes. Ovaries used to assess reproductive aging parameters were fixed for histological analysis in Modified Davidson's (Electron Microscopy Sciences, Hatfield, PA) at room temperature for 2-4 hours with agitation and overnight at 4°C. Ovaries used for MIMS were cut in half and fixed in 2% glutaraldehyde (Electron Microscopy Sciences, Hatfield, PA) and embedded in LR white (EMS). Ovaries used for LC-MS/MS were snap frozen and stored at -80°C until use.

To maximize the yield of a synchronized population of fully grown oocytes for LC-MS/MS, mice were hyperstimulated with an intraperitoneal injection of 5 IU pregnant mare serum gonadotropin (PMSG) (Prospec Bio, East Brunswick, N). Ovaries were harvested 44-48 hours post-PMSG injection and placed in L15-PVP supplemented with 0.025% milrinone to maintain oocyte meiotic arrest (Sigma-Aldrich, St. Louis, MO).

Cumulus-oocyte-complexes (COCs) were released by puncturing antral follicles with insulin syringes. Oocytes were mechanically denuded from cumulus cells using a 75 µm stripper tip and washed thoroughly in L15/PVP/PS before being snap frozen. For analysis of ovulated eggs, mice were hyperstimulated as described above with PMSG followed by superovulation induction 44-46 hours later with an intraperitoneal injection of 5 IU human chorionic gonadotropin (hCG)(Sigma, St. Louis, MO). COCs were then collected from the oviducts of each mice 14-16 hours post-hCG injection, and the number of ovulated eggs were counted.

Ovarian follicle counts and histological analysis

The decline in the number of ovarian follicles is a hallmark of reproductive aging (1). Therefore, we evaluated follicle counts in histological sections of ovaries as done previously (9). In brief, fixed ovaries were washed three times with 70% ethanol and processed, dehydrated, and paraffin embedded using an automated tissue processor (Leica Biosystems, Buffalo Grove, IL). After embedding, ovaries were serial sectioned with every 5th tissue section stained with hematoxylin and eosin (H&E). All H&E-stained tissue sections were digitally scanned at the University of Washington's Histology and Imaging Core using Hamamatsu-HT imaging system (Hamamatsu Photonics, Hamamatsu City, Japan) at 20X magnification. Scanned images were uploaded and visualized using the NDP.view2 software (Hamamatsu Photonics, Hamamatsu City, Japan). Follicles were classified and counted in every 5th tissue section. Follicles were classified by stage (primordial, primary, secondary, and antral) according to established criteria (9). Primordial follicles were comprised of an incomplete layer of squamous granulosa cells, while primary follicles contained a complete layer of cuboidal granulosa cells. Secondary follicles contained two or more layers of cuboidal granulosa cells. Antral follicles had more than eight layers of granulosa cells with the presence of an antrum, or fluid-filled cavity. All primordial and primary follicles were counted regardless of whether the oocyte's nucleus was visible. Secondary and antral follicles were counted only if the nucleus was visible to avoid double counting. Only healthy follicles were included in the final counts. Atretic follicles containing abnormally shaped oocytes with dark, pyknotic granulosa cells were excluded. The average number of follicles per area of ovarian section was calculated and used to compare counts between each age cohort.

Ovarian fibrosis, characterized by excess collagen, is another hallmark of reproductive aging (19). We evaluated fibrosis in ovaries by Picrosirius Red (PSR), a histological stain which detects collagen I and III (19). Ovarian tissue sections were deparaffinized in Citrisolv (Fisher Scientific, Pittsburgh, PA) and rehydrated in 100%, 70%, and 30% ethanol baths. Slides were submerged in

PSR staining solution composed of Sirius Red F3BA (Direct Red 80, C.I. 357.82, Sigma-Aldrich, St. Louis, MO) and picric acid (Sigma-Aldrich, St. Louis, MO) at 0.1% w/v for 40 minutes at room temperature. The slides were then incubated in acidified water made of 0.05 M hydrochloric acid (Fisher Scientific) for 90 seconds. Tissue sections were dehydrated in 100% ethanol baths, three times for 30-second incubations. After dehydration, slides were immersed in Citrisolv for five minutes and mounted with Cytoseal XYL (Fisher Scientific). PSR stained sections were then imaged with an EVOS FL Auto Imaging system (Thermo Fisher, Waltham, MA) using a 20X objective. Scans of whole ovarian tissue sections were performed to quantify the area of positive PSR staining using a threshold feature on ImageJ as previously described (Briley et. 2016). PSR positive staining was analyzed on two different ovarian tissue sections for three mice within each age cohort: 6 weeks, 6 months, and 10 months. Results were averaged to obtain average percent area of collagen.

Multi-isotope imaging mass spectrometry (MIMS) and data processing

Fixed LR white-embedded ovaries were sectioned to 0.5 microns and mounted on silicon wafers. At the Brigham and Women's Hospital Center for NanoImaging, a NanoSims 50L (CAMECA Instruments Inc., Madison, WI) instrument was tuned to simultaneously measure $^{12}C^{14}N^-$, $^{12}C^{15}N^-$, and $^{31}P^-$ secondary ions as described previously for imaging of a wide range of mouse and human tissues (56). Quantitative $^{12}C^{14}N$ images were used for histological representation of stereotypical ovarian structures and associated cell types. ^{31}P images provided additional histological detail and were used for identification of nuclei due to the high phosphorus content of chromatin (29). Quantitative mass images for $^{12}C^{14}N$ and $^{12}C^{15}N$ were used to generate quantitative ^{15}N:^{14}N ratio images. For imaging of swathes of the tissue section, images were acquired in chain analysis mode of sequential adjacent fields (dimensions of 45 µm x 45 µm or 50 µm x 50 µm). Sequential tiles were stitched together to make mosaic images for visualizing large sections of the ovary (**Fig. 1B**). Some features were then imaged at higher resolution with smaller field sizes. All images were processed and further analyzed using the most recent version of the OpenMIMS 2.0 plugin (*https://github.com/BWHCNI/OpenMIMS*) to ImageJ (57). ^{15}N-labeling was visualized by a hue saturation intensity (HSI) transformation of the $^{12}C^{15}N$/ $^{12}C^{14}N$ ratio. The color scale of HSI images is set such that the lower blue bound of the scale is at the ^{15}N natural abundance of 0.37% (expressed as 0 % above background). The upper magenta bound of the scale is set to reveal labeling differences. The quantitative isotope ratio measurements that form the basis for the images and that are used for statistical analyses are not affected by scaling changes that modify the visual appearance of the images (**fig. S2 A-B**). A combination of ^{14}N and ^{31}P images were used to manually select regions of interest within each ovarian section (e.g. individual cells or subcellular structures). Structures and cell types were identified based on morphology and their anatomic location. Cells that were not identifiable or were not visualized due to low ion counts were excluded from the analysis. Typical reasons for difficult identifying cells include sectioning artifacts (cracks, wrinkles) or certain cells that were located at the juncture between adjacent imaging fields, where there is often lower yield of secondary ions. This edge effect is seen to variable degrees in the mosaic images as dark regions at the periphery of an imaging field. All quantitative data for ^{15}N-labeling was presented as the $^{15}N/^{14}N$ ratio (percentage above natural abundance).

Mass Spectrometry (MS) sample preparation: ovaries

Isolated ovaries were homogenized directly in 6M guanidine hydrochloride solution using bead-based Precellys 24 homogenizer, followed by processing with ProteaseMAX according to manufacturer's protocol. Samples were reduced with 5 mM Tris(2-carboxyethyl)phosphine (TCEP; vortex 1 hr at RT) alkylated in the dark with 10 mM iodoacetamide (IAA; 20 min), diluted with 50 mM ABC and quenched with 25 mM TCEP. Samples were digested with sequencing grade modified trypsin overnight at 37°C with shaking, spun down (15,000 × g for 15 min at RT), placed in a new tube and acidified with TFA to a final concentration of 0.1%. A total of 100 µg of digested and acidified sample was fractionated using High pH Reversed-Phase Peptide Fractionation Kit (Pierce,

Cat# 84868). Fractions were step eluted in 300 µL buffer of increasing acetonitrile (ACN) concentrations with decreasing concentration of Triethylamine (0.1%) as per manufacturer. Samples were dried down with vacuum centrifugation for future MS analysis.

MS sample preparation: GeLC/MS on oocytes

Isolated oocytes were lysed directly in RIPA buffer, mixed with 6X SDS sample buffer, boiled for 5 minutes, and separated by SDS-PAGE using 10% Tris-glycine gels (Thermo Scientific, Cat# XV00100PK20). Gels were stained using Oriole fluorescent gel stain solution, scanned using Bio-rad Chemidoc XRS system, and cut into sections, chopped into 1mm x 1 mm cubes, and processed for in-gel digestion. The gel separating oocytes collected at t=6 months was cut into 36 individual pieces, whereas the gel separating oocytes collected at t=10 months was cut into 24 pieces. Gel pieces were incubated in 10 mM TCEP (in 50 mM ABC; 1 hr at 37 °C). Liquid was replaced by 50 mM IAA (in 50 mM ABC; 45 min at RT in dark), followed by 50 mM TCEP (in 50 mM ABC; 30 min at RT). Gel pieces were washed with 50 mM ABC (3x) and digested with sequencing grade modified trypsin (1 µg in 50 mM ABC, overnight at 37 °C, with shaking). The following day, supernatant was collected into new tube and the gel piece were subjected to three rounds of incubations with 50% ACN and 5% FA solution (30 min at RT, with shaking). Supernatant was collected after each incubation, combined, and dried down with vacuum centrifugation. Samples were re-suspended in 0.5% TFA, desalted with Pierce C18 spin columns (Thermo Scientific, Cat# 89873) per manufacturer's instructions, and dried down with vacuum centrifugation for future MS analysis.

MS analysis

Dried samples were re-suspended in 20 µL Buffer A (94.875% H2O with 5% ACN and 0.125% FA) and three micrograms, as determined by microBCA assay (Thermo Scientific, Cat# 23235) of each fraction or sample were loaded via auto-sampler with either Thermo EASY nLC 100 UPLC or UltiMate 3000 HPLC pump, onto a vented Pepmap 100, 75um x 2 cm, nanoViper trap column coupled to a nanoViper analytical column (Thermo Scientific) with stainless steel emitter tip assembled on the Nanospray Flex Ion Source with a spray voltage of 2000 V. A coupled Orbitrap Fusion was used to generate MS data. Buffer A contained 94.785% H_2O with 5% ACN and 0.125% FA, and buffer B contained 99.875 ACN with 0.125% FA. MS parameters were as follows: Ion transfer tube temp = 300 °C, Easy-IC internal mass calibration, default charge state = 2 and cycle time = 3 s. Detector type set to Orbitrap, with 60K resolution, with wide quad isolation, mass range = normal, scan range = 300-1500 m/z, max injection time = 50 ms, AGC target = 200,000, microscans = 1, S-lens RF level = 60, without source fragmentation, and datatype = positive and centroid. MIPS was set as on, included charge states = 2-6 (reject unassigned). Dynamic exclusion enabled with n = 1 for 30 s and 45 s exclusion duration at 10 ppm for high and low. Precursor selection decision = most intense, top 20, isolation window = 1.6, scan range = auto normal, first mass = 110, collision energy 30%, CID, Detector type = ion trap, OT resolution = 30K, IT scan rate = rapid, max injection time = 75 ms, AGC target = 10,000, Q=0.25, inject ions for all available parallelizable time. For ovary samples the chromatographic run was 4.5 hours per fraction, with the following profile of Buffer B: 2% for 7 min, 2-7% for 1 min, 7-10% for 5 min, 10-25% for 160 min, 25-33% for 40 min, 33-50% for 7 min, 50-95% for 5 min, 95% for 15 min, then back to 2% for the remaining 30 min. For the GeLC/MS oocyte samples, the chromatographic run was 75 min per gel section with the following profile of Buffer B: 2-8% for 6 min, 8-24% for 10 min, 24-36% for 20 min, 36-55% for 10 min, 55-95% for 10 min, 95% for 10 min, then back to 2% for remaining 9 min.

MS Data Analysis and Quantification

Protein identification/quantification and analysis were performed with Integrated Proteomics Pipeline - IP2 (Integrated Proteomics Applications, Inc., San Diego, CA. *http://www.integratedproteomics.com/*) using ProLuCID (58, 59), DTASelect2 (60, 61), Census and QuantCompare. Spectral raw files were extracted into MS1, MS2 files using RawConverter 1.0.0.0 (*http://fields.scripps.edu/downloads.php*). The tandem mass spectra were searched against mouse

database (downloaded on 03-25-2014). Searched spectra were matched to sequences using the ProLuCID/SEQUEST algorithm (ProLuCID version 3.1) with 50 ppm peptide mass tolerance for precursor ions and 600 ppm for fragment ions. ProLuCID searches included all fully and half-tryptic peptide candidates that fell within the mass tolerance window and had with unlimited mis-cleavages. Carbamidomethylation (+57.02146 Da) of cysteine was considered as a static modification. Peptide/spectrum matches (PSMs) were assessed in DTASelect2 using the cross-correlation score (XCorr), and normalized difference in cross-correlation scores (DeltaCN). Each protein identified was required to have a minimum of one peptide (-p1) of minimal length of six amino acid residues. False discovery rate (FDR) was set to 1% at the protein level, for all experiments. Peptide probabilities and FDR were calculated based on a target/decoy database containing the reversed sequences of all the proteins appended to the target database (62). Each dataset was searched twice, once against light (^{14}N) and then against heavy (^{15}N) protein databases, as described previously(14). In the light searches, all of the amino acid residues were considered to contain only ^{14}N nitrogen, while in the heavy searches, all the amino acid residues were considered to contain only ^{15}N nitrogen. After the results from ProLuCID were filtered using DTASelect2, and the assembled search result file was used to obtain quantitative ratios between ^{14}N and ^{15}N using the software Census (30, 63).

Long-lived proteins were identified as previously described, with modifications (14). Briefly, in order for a protein to be considered as long-lived, the protein had to be identified in our heavy/light search by at least one long-lived peptide (^{15}N-peptide). Peptide ratio measurements were filtered in Census based on a correlation threshold, and only peptides with correlation coefficient above 0.5 were used for further analysis. For singleton analysis, we required the ^{14}N/^{15}N ratio to be greater than 5.0 and the threshold score to be greater than 0.5. Identified peptides were further filtered based on their average peptide enrichment (APE), which we set to 0.9, and peptide profile score, which was set to 0.8. Proteins were only identified as long-lived if they had more than three long-lived peptides that passed the above filtering (except for GeLC/MS experiments where one peptide was required). Fractional abundance were calculated according to the following formula: ^{14}N values: FA = 100 – (100∗(1/(1+AR))), where FA = fractional abundance and AR = area ratio.

Gene Ontology Analysis

GO analysis was performed using the Pantherdb (64). The “query” is defined as proteins identified as long-lived in the analyzed tissue (based on ^{14}N-peptide identification), and the reference is defined as all proteins identified in the same tissue analyzed (^{14}N and ^{15}N-peptide identification).

Statistical analysis

Statistical analyses were conducted using GraphPad Prism, version 9 (GraphPad Software, Inc.). A Student’s t-test was performed for comparisons between two groups. For comparisons of more than two groups, a one-way ANOVA was used. A one sample t-test was used to compare ^{15}N/^{14}N ratios of cytoplasmic and nuclear regions to a hypothetical value of 1. Values >1 signified a cell had greater ^{15}N-labelling abundance in the nucleus compared to the cytoplasm. Values <1 represented cells with a lower ^{15}N-labelling abundance in the nucleus compared to the cytoplasm. Values equal to 1 represented a cell with a ^{15}N-labelling abundance that were equivalent in both nuclear and cytoplasmic regions. Data were considered significant with a p-value <.05 (* p-value <.05, ** p-value <.01, *** p-value <.001). Variability of groups was denoted as standard error of mean (SEM).

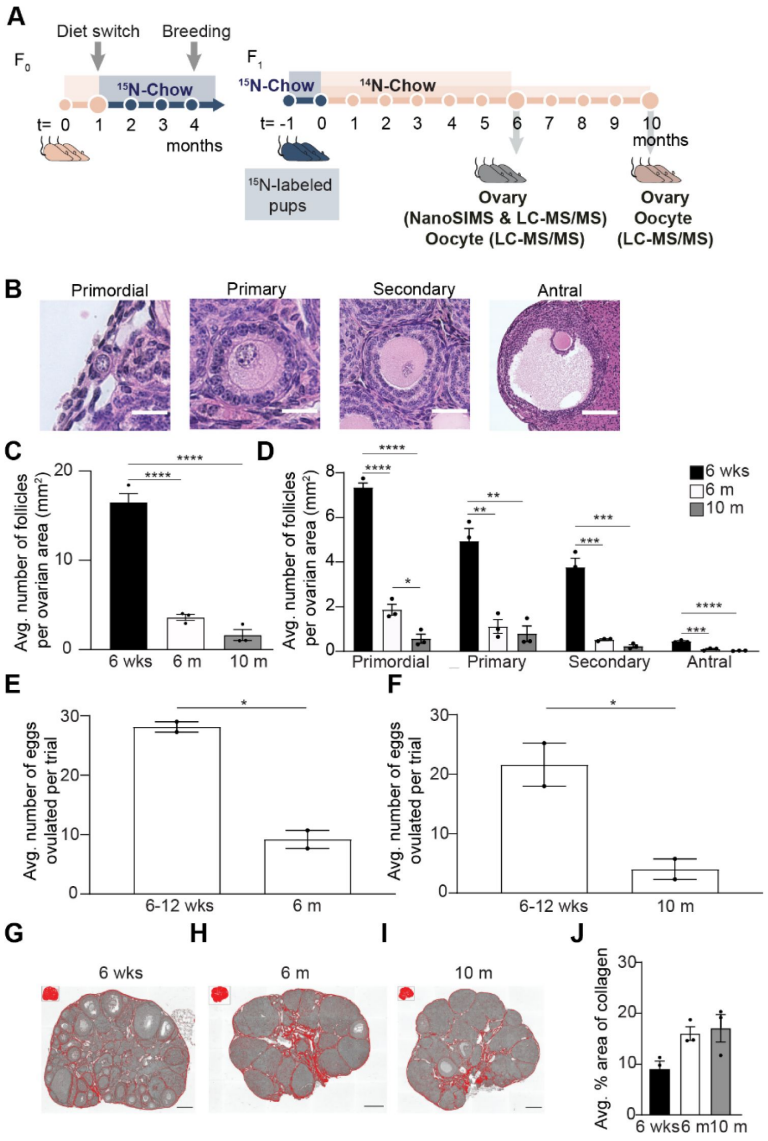

Fig. S1

Multi-generational whole animal pulse-chase labeling design along the reproductive aging continuum.

(A) Wild-type female FVB mice (n=3) were fed a ^{15}N-diet for 13 weeks and were maintained on a ^{15}N-labeled diet through breeding, pregnancy, and weaning to produce ^{15}N-labeled pups. Labeled pups were sacrificed after switching over to a ^{14}N-diet for a chase period of 6- or 10-months. Ovaries and oocytes were designated for NanoSIMS, or liquid-chromatography/mass spectrometry. Female FVB mice experience age-associated changes in ovarian reserve, ovarian microenvironment, and gamete quality. **(B)** Representative images of each follicle class from mice of 6 weeks old and 6 months old. **(C)** Average follicle number per area of ovarian section from mice of the following ages: 6 weeks, 6 months, and 10 months (N= 3 mice per age cohort). **(D)** Graph represents average number of follicles within each follicle class per area of ovarian section for mice ages 6 weeks, 6 months, and 10 months. (**E**) Comparison of average number of eggs ovulated per trial for mice at 6-12 wks, 6 months, and (**F**) 10 months. The data points represent the average number of eggs collected per mouse from two independent trials. In each trial, oviducts from 3-4 mice were pooled per age group. Representative processed color threshold images of PSR-stained ovarian tissue sections from mice **(G)** 6 weeks old, **(H)** 6 months old, and **(I)** 10 months old. **(J)** Graph comparing the average percent area of PSR-positive staining per ovarian section (pixels/μm^2). Data are shown as mean ± SEM. Statistical analysis was performed using a one-way ANOVA. Asterisk denotes statistical significance (* p≤.05; ** p≤.01; *** p≤.001; **** p≤.0001). Scale bar for images of (B) primordial, primary, secondary, and antral follicles are 20 μm, 40 μm, and 140 μm, respectively. Scale bars in (G-I) are 180 μm.

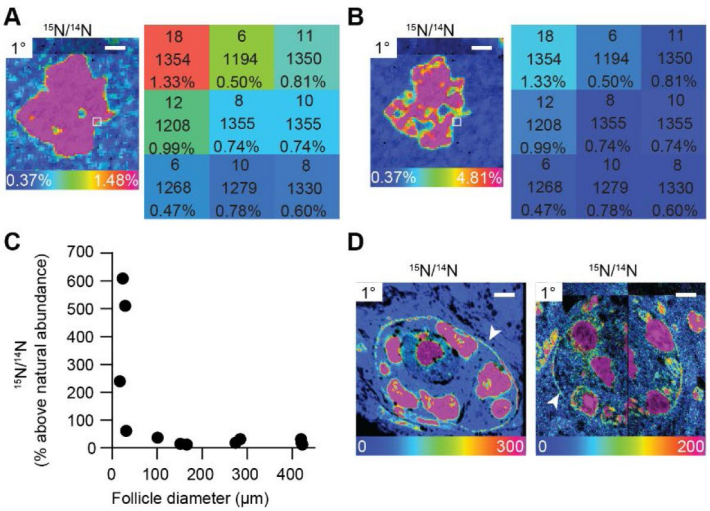

Fig. S2

Multi-isotope imaging mass spectrometry (MIMs) uncovers structures enriched with ^{15}N.

(A) Hue saturation intensity image maps $^{15}N/^{14}N$ ratio across nuclear region of a primary follicle. Using a rainbow scale, blue is set to the natural ratio of ^{15}N (0.37%) and overabundance is set to 1.48% (or 300% above the natural ratio). Each pixel provides quantitative information. The numbers in each pixel represent the number of ^{15}N ions, ^{14}N ions, and the $^{15}N/^{14}N$ ratio, respectively. (B) Changes to the rainbow scale can be used to emphasize regional ratio differences and change the visual representation of the data. Visual changes to HSI images due to different scales, does not change the quantitative data behind each pixel. (C) Total ^{15}N abundance of each follicle plotted by follicle diameter shows smaller follicles containing high abundance of ^{15}N. (D) HSI images reveal high ^{15}N abundance concentrated at the basement membrane of early-stage follicles. Scale bar (panel A-B) =2.5 µm, (D) left= 4.0 µm, (D) right = 4.5 µm.

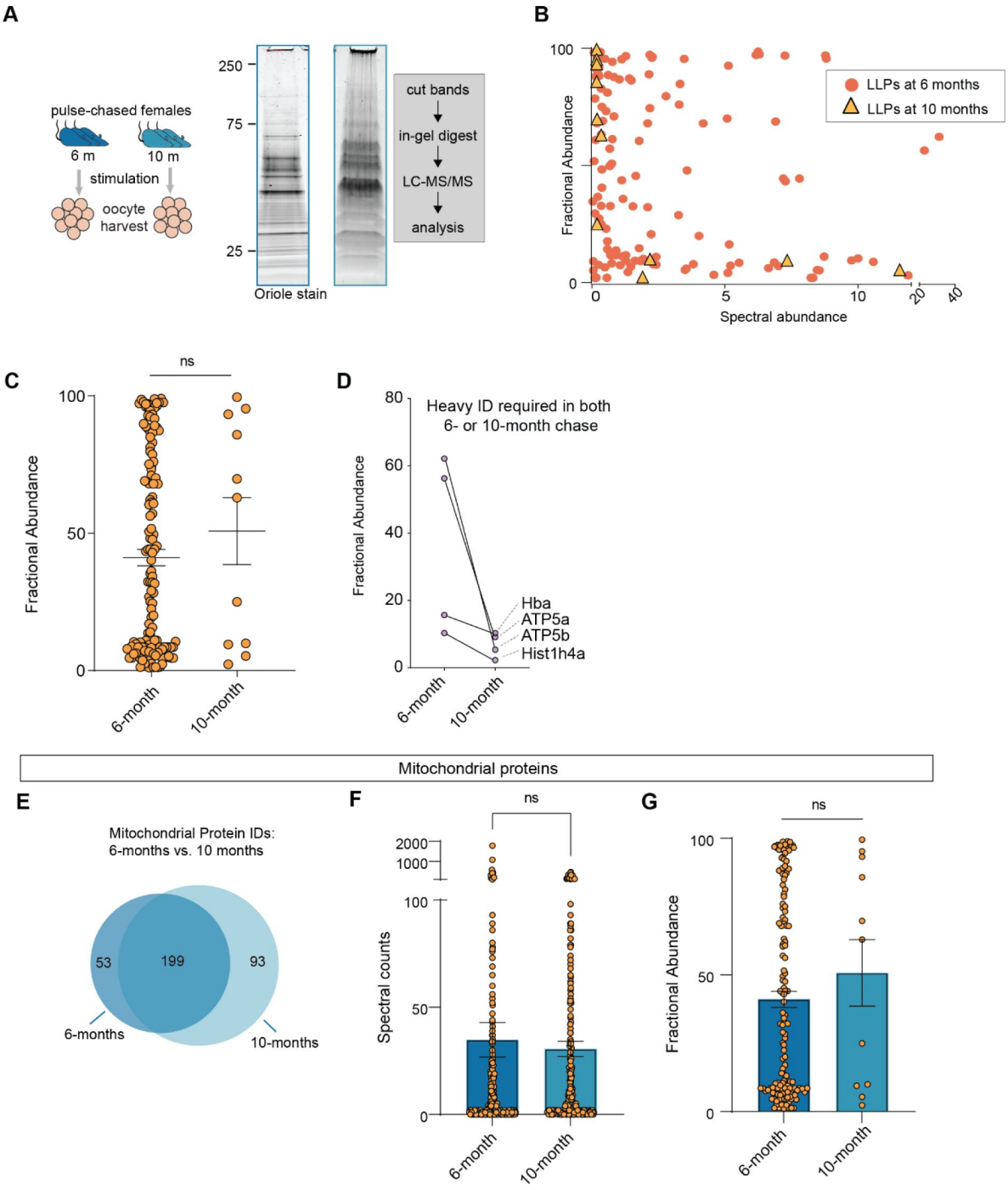

Fig. S3

Long-lived proteins at 6- and 10-months chase points in oocytes.

(A) Experimental scheme to identify and measure LLPs mouse oocyte. **(B-C)** Fractional abundance of each identified LLPs at both 6 months and 10 months as compared to the spectral abundance for each LLPs. **(D)** Plots showing decrease in FA values for same proteins identified as LLPs at 6 and 10-month chase. (E) Venn diagram illustrating the overlap of mitochondrial proteins identified at 6 and 10-month time points (F) Spectral counts of mitochondrial proteins as well as the (G) fractional abundance of each identified mito-LLPs at both 6 months and 10 months, illustrating that even though there are no significant difference in spectral counts at each timepoint, the number of quantified proteins decreased dramatically between 6 and 10 months of chase.

References

1. Broekmans F. J., Soules M. R., Fauser B. C. (2009) **Ovarian aging: mechanisms and clinical consequences** *Endocrine reviews* **30**:465–493

2. Reefhuis J., Honein M. A. (2004) **Maternal age and non-chromosomal birth defects** *Atlanta--1968-2000: teenager or thirty-something, who is at risk? Birth defects research. Part A, Clinical and molecular teratology* **70**

3. Mai C. T., et al. (2013) **Selected birth defects data from population-based birth defects surveillance programs in the United States, 2006 to 2010: featuring trisomy conditions** *Birth defects research. Part A, Clinical and molecular teratology* **97**

4. Hollier L. M., Leveno K. J., Kelly M. A., F. G. Cunningham M. C. DD (2000) **Maternal age and malformations in singleton births** *Obstetrics and gynecology* **96**:701–706

5. Johnson J. A., Tough S., Society of O., Gynaecologists of C. (2012) **Delayed child-bearing** *J Obstet Gynaecol Can* **34**:80–93

6. Buyuk E., Nejat E., Neal-Perry G. (2010) **Determinants of female reproductive senescence: differential roles for the ovary and the neuroendocrine axis** *Semin Reprod Med* **28**:370–379

7. Sauer M. V. (2015) **Reproduction at an advanced maternal age and maternal health** *Fertil Steril* **103**:1136–1143

8. Balasch J., Gratacos E. (2012) **Delayed childbearing: effects on fertility and the outcome of pregnancy** *Curr Opin Obstet Gynecol* **24**:187–193

9. Duncan F. E., et al. (2017) **Age-associated dysregulation of protein metabolism in the mammalian oocyte** *Aging Cell* **16**:1381–1393

10. Basisty N., Meyer J. G., Schilling B. (2018) **Protein Turnover in Aging and Longevity** *Proteomics* **18**

11. Fornasiero E. F., et al. (2018) **Precisely measured protein lifetimes in the mouse brain reveal differences across tissues and subcellular fractions** *Nat Commun* **9**

12. Fornasiero E. F., Savas J. N. (2023) **Determining and interpreting protein lifetimes in mammalian tissues** *Trends Biochem Sci* **48**:106–118

13. Bomba-Warczak E., Edassery S. L., Hark T. J., Savas J. N. (2021) **Long-lived mitochondrial cristae proteins in mouse heart and brain** *J Cell Biol* **220**

14. Savas J. N., Toyama B. H., Xu T., Yates J. R. (2012) **3rd, M. W. Hetzer, Extremely long-lived nuclear pore proteins in the rat brain** *Science* **335**

15. Toyama B. H., et al. (2013) **Identification of long-lived proteins reveals exceptional stability of essential cellular structures** *Cell* **154**:971–982

16. Bomba-Warczak E., Savas J. N. (2022) **Long-lived mitochondrial proteins and why they exist** *Trends Cell Biol* **32**:646–654

17. Hunt P. A., Hassold T. J. (2008) **Human female meiosis: what makes a good egg go bad?** *Trends Genet* **24**:86–93

18. Nagaoka S. I., Hassold T. J., Hunt P. A. (2012) **Human aneuploidy: mechanisms and new insights into an age-old problem** *Nat Rev Genet* **13**:493–504

19. Amargant F., et al. (2020) **Ovarian stiffness increases with age in the mammalian ovary and depends on collagen and hyaluronan matrices** *Aging Cell* **19**

20. Briley S. M., et al. (2016) **Reproductive age-associated fibrosis in the stroma of the mammalian ovary** *Reproduction* **152**:245–260

21. Machlin J. H., et al. (2021) **Fibroinflammatory Signatures Increase with Age in the Human Ovary and Follicular Fluid** *Int J Mol Sci* **22**

22. Kinnear H. M., et al. (2020) **The ovarian stroma as a new frontier** *Reproduction* **160**:R25–R39

23. Kimler B. F., et al. (2018) **Radiation-induced ovarian follicle loss occurs without overt stromal changes** *Reproduction* **155**:553–562

24. Perrone R., et al. (2023) **CD38 regulates ovarian function and fecundity via NAD(+) metabolism** *iScience* **26**

25. Quan N., et al. (2020) **Differential sensitivity of inbred mouse strains to ovarian damage in response to low-dose total body irradiationdagger** *Biol Reprod* **102**:133–144

26. Steinhauser M. L., Lechene C. P. (2013) **Quantitative imaging of subcellular metabolism with stable isotopes and multi-isotope imaging mass spectrometry** *Semin Cell Dev Biol* **24**:661–667

27. Guillermier C., Steinhauser M. L., Lechene C. P. (2014) **Quasi-simultaneous acquisition of nine secondary ions with seven detectors on NanoSIMS50L: application to biological samples** *Surf Interface Anal* **46**:150–153

28. Nunez J., Renslow R., Cliff J. B. (2017) **3rd, C. R. Anderton, NanoSIMS for biological applications: Current practices and analyses** *Biointerphases* **13**

29. Guillermier C., et al. (2017) **Imaging mass spectrometry demonstrates age-related decline in human adipose plasticity** *JCI Insight* **2**

30. Park S. K., Venable J. D., Xu T., Yates J. R. (2008) **3rd, A quantitative analysis software tool for mass spectrometry-based proteomics** *Nat Methods* **5**:319–322

31. Rodriguez-Nuevo A., et al. (2022) **Oocytes maintain ROS-free mitochondrial metabolism by suppressing complex I** *Nature* **607**:756–761

32. Oktay K., Briggs D., Gosden R. G. (1997) **Ontogeny of follicle-stimulating hormone receptor gene expression in isolated human ovarian follicles** *J Clin Endocrinol Metab* **82**:3748–3751

33. Szotek P. P., et al. (2008) **Normal ovarian surface epithelial label-retaining cells exhibit stem/progenitor cell characteristics** *Proc Natl Acad Sci U S A* **105**:12469–12473

34. Thayer N. H., et al. (2014) **Identification of long-lived proteins retained in cells undergoing repeated asymmetric divisions** *Proc Natl Acad Sci U S A* **111**:14019–14026

35. Mara J. N., et al. (2020) **Ovulation and ovarian wound healing are impaired with advanced reproductive age** *Aging (Albany NY* **12**:9686–9713

36. Paulini F., Silva R. C., Rolo J. L., Lucci C. M. (2014) **Ultrastructural changes in oocytes during folliculogenesis in domestic mammals** *J Ovarian Res* **7**

37. Eppig J. J., Wigglesworth K., Pendola F. L. (2002) **The mammalian oocyte orchestrates the rate of ovarian follicular development** *Proc Natl Acad Sci U S A* **99**:2890–2894

38. Grootenhuis A. J., Philipsen H. L., de Breet-Grijsbach J. T., van Duin M. (1996) **Immunocytochemical localization of ZP3 in primordial follicles of rabbit, marmoset, rhesus monkey and human ovaries using antibodies against human ZP3** *J Reprod Fertil Suppl* **50**:43–54

39. Gook D. A., Edgar D. H., Borg J., Martic M. (2008) **Detection of zona pellucida proteins during human folliculogenesis** *Hum Reprod* **23**:394–402

40. Henning N. F., LeDuc R. D., Even K. A., Laronda M. M. (2019) **Proteomic analyses of decellularized porcine ovaries identified new matrisome proteins and spatial differences across and within ovarian compartments** *Sci Rep* **9**

41. Chiang T., Duncan F. E., Schindler K., Schultz R. M., Lampson M. A. (2010) **Evidence that Weakened Centromere Cohesion Is a Leading Cause of Age-Related Aneuploidy in Oocytes** *Curr Biol* **20**:1522–1528

42. Dong J., et al. (2023) **Ectopic expression of human TUBB8 leads to increased aneuploidy in mouse oocytes** *Cell Discov* **9**

43. Feng R., et al. (2016) **Mutations in TUBB8 and Human Oocyte Meiotic Arrest** *N Engl J Med* **374**:223–232

44. Nashun B., et al. (2015) **Continuous Histone Replacement by Hira Is Essential for Normal Transcriptional Regulation and De Novo DNA Methylation during Mouse Oogenesis** *Mol Cell* **60**:611–625

45. Uraji J., Scheffler K., Schuh M. (2018) **Functions of actin in mouse oocytes at a glance** *J Cell Sci* **131**

46. Duan X., Sun S. C. (2019) **Actin cytoskeleton dynamics in mammalian oocyte meiosis** *Biol Reprod* **100**:15–24

47. Roeles J., Tsiavaliaris G. (2019) **Actin-microtubule interplay coordinates spindle assembly in human oocytes** *Nat Commun* **10**

48. Ajduk A., et al. (2011) **Rhythmic actomyosin-driven contractions induced by sperm entry predict mammalian embryo viability** *Nat Commun* **2**

49. Dunkley S., Scheffler K., Mogessie B. (2022) **Cytoskeletal form and function in mammalian oocytes and zygotes** *Curr Opin Cell Biol* **75**

50. Diaz H., Esponda P. (2004) **Ageing-induced changes in the cortical granules of mouse eggs** *Zygote* **12**:95–103

51. van der Reest J., Cecchino G. N., Haigis M. C., Kordowitzki P. (2021) **Mitochondria: Their relevance during oocyte ageing** *Ageing Res Rev* **70**

52. Kujoth G. C., et al. (2005) **Mitochondrial DNA mutations, oxidative stress, and apoptosis in mammalian aging** *Science* **309**:481–484

53. Wai T., et al. (2010) **The role of mitochondrial DNA copy number in mammalian fertility** *Biol Reprod* **83**:52–62

54. Babayev E., Seli E. (2015) **Oocyte mitochondrial function and reproduction** *Curr Opin Obstet Gynecol* **27**:175–181

55. Chiaratti M. R., et al. (2018) **The role of mitochondria in the female germline: Implications to fertility and inheritance of mitochondrial diseases** *Cell Biol Int* **42**:711–724

56. Steinhauser M. L., et al. (2012) **Multi-isotope imaging mass spectrometry quantifies stem cell division and metabolism** *Nature* **481**:516–519

57. Guillermier C., Poczatek J. C., Taylor W. R., Steinhauser M. L. (2017) **Quantitative imaging of deuterated metabolic tracers in biological tissues with nanoscale secondary ion mass spectrometry** *Int J Mass Spectrom* **422**:42–50

58. Eng J. K., McCormack A. L., Yates J. R. (1994) **An approach to correlate tandem mass spectral data of peptides with amino acid sequences in a protein database** *J Am Soc Mass Spectrom* **5**:976–989

59. Xu T., et al. (2015) **ProLuCID: An improved SEQUEST-like algorithm with enhanced sensitivity and specificity** *J Proteomics* **129**:16–24

60. Cociorva D., J. R. Yates L. T. D (2007) **Validation of tandem mass spectrometry database search results using DTASelect** *Curr Protoc Bioinformatics* **16**:13–13

61. Tabb D. L., McDonald W. H., Yates J. R. (2002) **3rd, DTASelect and Contrast: tools for assembling and comparing protein identifications from shotgun proteomics** *J Proteome Res* **1**:21–26

62. Peng J., Elias J. E., Thoreen C. C., Licklider L. J., Gygi S. P. (2003) **Evaluation of multidimensional chromatography coupled with tandem mass spectrometry (LC/LC-MS/MS) for large-scale protein analysis: the yeast proteome** *J Proteome Res* **2**:43–50

63. MacCoss M. J., Wu C. C., Liu H., Sadygov R., Yates J. R. (2003) **3rd, A correlation algorithm for the automated quantitative analysis of shotgun proteomics data** *Anal Chem* **75**:6912–6921

64. Mi H., Muruganujan A., Ebert D., Huang X., Thomas P. D. (2019) **PANTHER version 14: more genomes, a new PANTHER GO-slim and improvements in enrichment analysis tools** *Nucleic Acids Res* **47**:D419–D426

Editors

Reviewing Editor
Darryl Russell
University of Adelaide, Adelaide, Australia

Senior Editor
Wei Yan
The Lundquist Institute, Torrance, United States of America

Reviewer #1 (Public Review):

Summary:

This manuscript by Bomba-Warczak describes a comprehensive evaluation of long-lived proteins in the ovary using a transgenerational diet-derived 15N-labelling in pulse-chased mice. The transgenerational labeling of proteins (and nucleic acids) with 15N allowed the authors to identify regions enriched in long-lived macromolecules at the 6 and 10-month chase time points. The authors also identified the retained proteins in the ovary and oocyte using MS. Key findings include the relative enrichment in long-lived macromolecules in oocytes, pregranulosa cells, CL, stroma, and surprisingly OSE. Gene ontology analysis of these proteins revealed an enrichment for nucleosome, myosin complex, mitochondria, and other matrix-type protein functions. Interestingly, compared to other post-mitotic tissues where such analyses have been previously performed such as the brain and heart, they find a higher fractional abundance of labeled proteins related to the mitochondria and myosin respectively.

Strengths:

A major strength of the study is the combined spatial analyses of LLPs using histological sections with MS analysis to identify retained proteins.

Another major strength is the use of two chase time points allowing assessment of temporal changes in LLPs associated with aging.

The major claims such as an enrichment of LLPs in pregranulosa cells, GCs of primary follicles, CL, stroma, and OSE are soundly supported by the analyses and the caveat that nucleic acids might differentially contribute to this signal is well presented.

The claims that nucleosomes, myosin complex, and mitochondrial proteins are enriched for LLPs are well supported by GO enrichment analysis and well described within the known body of evidence that these proteins are generally long-lived in other tissues.

Weaknesses:

All weaknesses were addressed in the revised manuscript.

Impact of the work:

This work represents the first study addressing the turnover and retention of long-lived protein in the ovary and will be an invaluable resource for the research community, particularly for those studying ovarian aging. This work also raises important unanswered questions worthy of follow-up including interesting findings regarding the timing of turnover of cell types such as the OSE, organelles such as mitochondria, and ECM proteins such as ZP3 and Tubb family proteins. Most striking are the differences between the two timepoints used (6 and 10 months) which lead the authors to infer trajectories and kinetics of replacement of

proteins potentially contributing to ovarian longevity or decline. As such I expect the work will contribute to hypothesis generation and stand to have an important impact on the field.

https://doi.org/10.7554/eLife.93172.2.sa3

Reviewer #2 (Public Review):

Summary:

The manuscript by Bomba-Warczak et al. applied multi-isotope imaging mass spectrometry (MIMS) analysis to identify the long-lived proteins in mouse ovaries during reproductive aging, and found some proteins related to cytoskeletal and mitochondrial dynamics persisting for 10 months.

Strengths:

The manuscript provides a useful dataset about protein turnover during ovarian aging in mice.

Weaknesses:

The study is pretty descriptive and short of further new findings based on the dataset. In addition, some results such as the numbers of follicles and ovulated oocytes in aged mice are not consistent with the published literature.

Comments on revised version:

The authors did not fully address my previous concerns, especially regarding the verification of the identified proteins, and follow-up functional experiments. In addition, it is still unacceptable for me that the number of ovulated oocytes in mice at 6 months of age is only one third of young mice (10 vs 30; Fig. S1E). The most of published literature show that mice at 12 months of age still have ~10 ovulated oocytes. Moreover, based on the follicle counting method used in the present study (Fig. S1D), there are no antral follicles observed in mice at 6 months and 10 months of age, which is not reasonable.

https://doi.org/10.7554/eLife.93172.2.sa2

Reviewer #3 (Public Review):

Summary:

In this study Bomba-Warczak et al focused on the reproductive aging, and they presented a map for long-lived proteins which were stable during the reproductive lifespan. The authors used MIMS to examine and show distinct molecules in different cell types in the ovary and tissue regions in 6 months mice, and they also used proteomic analysis to present different LLPs in ovaries between these two timepoints in 6 months and 10 months mice; besides, the authors also examined the LLPs in oocytes in 6 months mice and indicated that these were nuclear, cytoskeleton and mitochondria proteins.

Strengths:

Overall, this study provided important information about the pattern of long-lived proteins during aging, which will contribute to the understanding of the defects caused by reproductive aging.

Weaknesses:

12 months mice were not examined as the typical aged model.

Comments on revised version:

The authors responded to my comments and suggestions. Due to the limitation of the manuscript type, most suggestions of my comments in first round could be considered for future studies by the authors.

https://doi.org/10.7554/eLife.93172.2.sa1

Author response:

The following is the authors' response to the current reviews.

> ***Reviewer 2:***
>
> *In addition, it is still unacceptable for me that the number of ovulated oocytes in mice at 6 months of age is only one third of young mice (10 vs 30; Fig. S1E). The most of published literature show that mice at 12 months of age still have ~10 ovulated oocytes.*

We disagree with the reviewer's comment, and the concerns raised were not shared by the other reviewers. We have reported our data with full transparency (each data point is plotted). In the current study, we observed an intermediate phenotype in gamete number (assessed by both ovarian follicle counts and ovulated eggs) when comparing 6 month old mice to 6 week or 10 month old mice; this is as expected. It is well accepted that follicle counts are highly mouse strain dependent. Although the reviewer mentions that mice at 12 months have ~10 ovulated oocytes, no actual references are provided nor are the mouse strain or other relevant experimental details mentioned. Therefore, we do not know how these quoted metrics relate to the female FVB mice used in our current study. As clearly explained and justified in our manuscript, we used mice at 6 months and 10 months to represent a physiologic aging continuum.

> *Moreover, based on the follicle counting method used in the present study (Fig. S1D), there are no antral follicles observed in mice at 6 months and 10 months of age, which is not reasonable.*

This statement is incorrect. Antral follicles were present at 6 and 10 months of age, but due to the scale of the y-axis and the normalization of follicle number/area in Fig. S1D, the values are small. The absolute number of antral follicles per ovary (counted in every 5th section) was 31.3 ± 3.8 follicles for 6-week old mice, 9.3 ± 2.3 follicles for 6-month old mice, and 5.3 ± 1.8 follicles for 10-month old mice. Moreover, it is important to note that these ovaries were not collected in a specific stage of the estrous cycle, so the number of antral follicles may not be maximal. In addition, as described in the Materials and Methods, antral follicles were only counted when the oocyte nucleus was present in a section to avoid double counting. Therefore, this approach (which was applied consistently across samples) could potentially underestimate the total number.

The following is the authors' response to the original reviews.

> ***Public Reviews:***
>
> ***Reviewer #1 (Public Review):***
>
> *Summary:*

> *This manuscript by Bomba-Warczak describes a comprehensive evaluation of long-lived proteins in the ovary using transgenerational radioactive labelled 15N pulse-chase in mice. The transgenerational labeling of proteins (and nucleic acids) with 15N allowed the authors to identify regions enriched in long-lived macromolecules at the 6 and 10-month chase time points. The authors also identify the retained proteins in the ovary and oocyte using MS. Key findings include the relative enrichment in long-lived macromolecules in oocytes, pregranulosa cells, CL, stroma, and surprisingly OSE. Gene ontology analysis of these proteins revealed enrichment for nucleosome, myosin complex, mitochondria, and other matrix-type protein functions. Interestingly, compared to other post-mitotic tissues where such analyses have been previously performed such as the brain and heart, they find a higher fractional abundance of labeled proteins related to the mitochondria and myosin respectively.*

Response: We thank the reviewer for this thoughtful summary of our work. We want to clarify that our pulse-chase strategy relied on a two-generation stable isotope-based metabolic labelling of mice using 15N from spirulina algae (for reference, please see (Fornasiero & Savas, 2023; Hark & Savas, 2021; Savas et al., 2012; Toyama et al., 2013)). We did not utilize any radioactive isotopes.

> *Strengths:*
>
> *A major strength of the study is the combined spatial analyses of LLPs using histological sections with MS analysis to identify retained proteins.*
>
> *Another major strength is the use of two chase time points allowing assessment of temporal changes in LLPs associated with aging.*
>
> *The major claims such as an enrichment of LLPs in pregranulosa cells, GCs of primary follicles, CL, stroma, and OSE are soundly supported by the analyses, and the caveat that nucleic acids might differentially contribute to this signal is well presented.*
>
> *The claims that nucleosomes, myosin complex, and mitochondrial proteins are enriched for LLPs are well supported by GO enrichment analysis and well described within the known body of evidence that these proteins are generally long-lived in other tissues.*
>
> *Weaknesses:*
>
> *Comment 1: One small potential weakness is the lack of a mechanistic explanation of if/why turnover may be accelerating at the 6-10 month interval compared to 1-6.*

Response 1: At the 6-month time point, we detected more long lived proteins than the 10 month time point in both the ovary and the oocyte. We anticipated this because proteins are degraded over time, and substantially more time has elapsed at the later time point. Moreover, at the 6–10-month time point, age-related tissue dysfunction is already evident in the ovary. For example, in 6-9 month old mice, there is already a deterioration of chromosome cohesion in the egg which results in increased interkinetochore distances (Chiang et al., 2010), and by 10 months, there are multinucleated giant cells present in the ovarian stroma which is consistent with chronic inflammation (Briley et al., 2016). Thus, the observed changes in protein dynamics may be another early feature of aging progression in the ovary.

> *Comment 2: A mild weakness is the open-ended explanation of OSE label retention. This is a very interesting finding, and the claims in the paper are nuanced and perfectly reflect the current understanding of OSE repair. However, if the sections are available and one could look at the spatial distribution of OSE signal across the ovarian surface it*

> *would interesting to note if label retention varied by regions such as the CLs or hilum where more/less OSE division may be expected.*

Response 2: We agree that the enrichment of long-lived molecules in the OSE is interesting. To make interpretable conclusions about the dynamics of long-lived molecules in the OSE, we would need to generate a series of samples at precise stages of the estrous cycle or ideally across a timecourse of ovulation to capture follicular rupture and repair. These samples do not currently exist and are beyond the scope of this study. However, this idea is an important future direction and it has been added to the discussion (lines 221-223). Furthermore, from a practical standpoint, MIMS imaging is resource and time intensive. Thus, we are not able to readily image entire ovarian sections. Instead, we focused on structures within the ovary and took select images of follicles, stroma, and OSE. We, therefore, do not have a comprehensive series of images of the OSE from the entire ovarian section for each mouse analyzed.

> ***Reviewer #2 (Public Review):***
>
> *Summary:*
>
> *The manuscript by Bomba-Warczak et al. applied multi-isotope imaging mass spectrometry (MIMS) analysis to identify the long-lived proteins in mouse ovaries during reproductive aging, and found some proteins related to cytoskeletal and mitochondrial dynamics persisting for 10 months.*

Response: We thank the reviewer for their summary and feedback.

> *Strengths:*
>
> *The manuscript provides a useful dataset about protein turnover during ovarian aging in mice.*
>
> *Weaknesses:*
>
> *Comment 1: The study is pretty descriptive and short of further new findings based on the dataset. In addition, some results such as the numbers of follicles and ovulated oocytes in aged mice are not consistent with the published literature, and the method for follicle counting is not accurate. The conclusions are not fully supported by the presented evidence.*

Response 1: We agree with the reviewer that this study is descriptive. Our goal, as stated, was to use a discovery-based approach to define the long-lived proteome of the ovary and oocyte across a reproductive aging continuum. As the prominent aging researcher, Dr. James Kirkland, stated: “although ‘descriptive’ is sometimes used as a pejorative term…descriptive or discovery research leading to hypothesis generation has become highly sophisticated and of great relevance to the aging field (Kirkland, 2013).” We respectfully disagree with the reviewer that our study is short of new findings. In fact, this is the first time that a stable two-generation stable isotope-based metabolic labelling of mice in combination with two different state-of-the-art mass spectrometry methods has been used to identify and localize long lived molecules in the ovary and oocyte along this particular reproductive aging continuum in an unbiased manner. We have identified proteins groups that were previously not known to be long lived in the ovary and oocyte. Our hope is that this long-lived proteome will become an important hypothesis-generating resource for the field of reproductive aging.

The age-dependent decline in number of follicles and eggs ovulated in mice has been well established by our group as well as others (Duncan et al., 2017; Mara et al., 2020). Thus, we are unclear about the reviewer’s comments that our results are not consistent with the published literature. The absolute numbers of follicles and eggs ovulated as well as the rate of

decline with age are highly strain dependent. Moreover, mice can have a very small ovarian reserve and still maintain fertility (Kerr et al., 2012). In our study, we saw a consistent age-dependent decrease in the ovarian reserve (Figure 1 – figure supplement 1 D), the number of oocytes collected from large antral follicles following hyperstimulation with PMSG (used for LC-MS/MS), and the number of eggs collected from the oviduct following hyperstimulation and superovulation with PMSG and hCG (Figure 1 – figure supplement 1 E and F). In all cases, the decline was greater in 10 month old compared to 6 month old mice demonstrating a relative reproductive aging continuum even at these time points.

Our research team has significant expertise in follicle classification and counting as evidenced by our publication record (Duncan et al., 2017; Kimler et al., 2018; Perrone et al., 2023; Quan et al., 2020). We used our established methods which we have further clarified in the manuscript text (lines 395-397). Follicle counts were performed on every 5th tissue section of serial sectioned ovaries, and 1 ovary from 3 mice per timepoint were counted. Therefore, follicle counts were performed on an average of 48-62 total sections per ovary. The number of follicles was then normalized per total area (mm2) of the tissue section, and the counts were averaged. Figure 1 – figure supplement 1 C and D represents data averaged from all ovarian sections counted per mouse. It is important to note that the same criteria were applied consistently to all ovaries across the study, and thus regardless of the technique used, the relative number of follicles or oocytes across ages can be compared.

> ***Reviewer #3 (Public Review):***
>
> *Summary:*
>
> *In this study, Bomba-Warczak et al focused on reproductive aging, and they presented a map for long-lived proteins that were stable during reproductive lifespan. The authors used MIMS to examine and show distinct molecules in different cell types in the ovary and tissue regions in a 6 month mice group, and they also used proteomic analysis to present different LLPs in ovaries between these two timepoints in 6-month and 10-month mice. The authors also examined the LLPs in oocytes in the 6-months mice group and indicated that these were nuclear, cytoskeleton, and mitochondria proteins.*

Response: We thank the reviewer for their summary and feedback.

> *Strengths:*
>
> *Overall, this study provided basic information or a 'map' of the pattern of long-lived proteins during aging, which will contribute to the understanding of the defects caused by reproductive aging.*
>
> *Weaknesses:*
>
> *Comment 1: The 6-month mice were used as an aged model; no validation experiments were performed with proteomics analysis only.*

Response 1: We did not select the 6-month time point to be representative of the “aged model” but rather one of two timepoints on the reproductive aging continuum – 6 and 10 months. In the manuscript (Figure 1 – figure supplement 1) we have demonstrated the relevance of the two timepoints by illustrating a decrease in follicle counts, number of fully grown oocytes collected, and number of eggs ovulated as well as a tendency towards increased stromal fibrosis (highlighted in the main text lines 78-85). Inclusion of the 6-month timepoint ultimately turned out to be informative and essential as many long-lived proteins were absent by the 10 month timepoint. These results suggest that important shifts in the proteome occur during mid to advanced reproductive age. The relevance of these timepoints is mentioned in the discussion (lines 247-270).

> *Two independent mass spectrometry approaches (MIMS and LC-MS/MS) were used to validate the presence of long-lived macromolecules in the ovary and oocyte. Studies focused on the role of specific long-lived proteins in oocyte and ovarian biology as well as how they change with age in terms of function, turnover, and modification are beyond the scope of the current study but are ongoing. We have acknowledged these important next steps in the manuscript text (lines 286-288, 311-312).*

It is important to note, that oocytes are biomass limited cells, and their numbers decrease with age. Thus, we had to select ages where we could still collect enough from the mice available to perform LC-MS/MS.

> *Recommendations for the authors:*
>
> *Reviewer #1 (Recommendations For The Authors):*
>
> *Comment 1: The writing and figures are beautiful - it would be hard to improve this manuscript.*

Response 1: We greatly appreciate this enthusiastic evaluation of our work.

> *Comment 2: In Fig S1E/F it would help to list the N number here. Why are there 2 groups at 6-12 wk?*

Response 2: We did not have 6 month and 10-month-old mice available at the same time to be able to run the hyperstimulation and superovulation experiment in parallel. Therefore, we performed independent experiments comparing the number of eggs collected from either 6-month-old or 10 month old mice relative to 6-12 week old controls. In each trial, eggs were collected from pooled oviducts from between 3-4 mice per age group, and the average total number of eggs per mouse was reported. Each point on the graph corresponds to the data from an individual trial, and two trials were performed. This has been clarified in the figure legend (lines 395-397). Of note, while addressing this reviewer's comments, we noticed that we were missing Materials and Methods regarding the collection of eggs from the oviduct following hyperstimulation and superovulation with PMSG and hCG. This information has now been added in Methods Section, lines 477-481.

> *Comment 3: The manuscript would benefit from an explanation of why the pups were kept on a 1-month N15 diet after birth, since the oocytes are already labeled before birth, and granulosa at most by day 3-4. Would ZP3 have not been identified otherwise?*

Response 3: The pups used in this study were obtained from fully labeled female dams that were maintained on an15N diet. These pups had to be kept with their mothers through weaning. To limit the pulse period only through birth, the pups would have had to be transferred to unlabeled foster mothers. However, this would have risked pup loss which would have significantly impacted our ability to conduct the studies given that we only had 19 labeled female pups from three breeding pairs. We have clarified this in the manuscript text in lines 78-80. It is hard to know, without doing the experiment, whether we would have detected ZP3 if we only labeled through birth. The expression of ZP3 in primordial follicles, albeit in human, would suggest that this protein is expressed quite early in development.

> *Comment 4: What is happening to the mitochondria at 6-10 months? Does their number change in the oocyte? Is there a change in the rate of fission? Any chance to take a stab at it with these or other age-matched slides?*

Response 4: The reviewer raises an excellent point. As mentioned previously in the Discussion (lines 290-301), there are well documented changes in mitochondrial structure and function in the oocyte in mice of advanced reproductive age. However, there is a paucity of data on the changes that may happen at earlier mid-reproductive age time points. From the oocyte mitochondrial proteome perspective, our data demonstrate a prominent decline in the persistence of long-lived proteins between 6 and 10 months, and this occurs in the absence of a change in the total pool of mitochondrial proteins (both long and short lived populations) as assessed by spectral counts or protein IDs (figure below). These data, which we have added into Figure 3 – figure supplement 1 and in the manuscript text (lines 164-170) are suggestive of similar numbers of mitochondria at these two timepoints. It would be informative to do a detailed characterization of oocyte mitochondrial structure and function within this window to see if there is a correlation with this shift in long lived mitochondrial proteins. Although this analysis is beyond the scope of the current manuscript, it is an important next line of inquiry which we have highlighted in the manuscript text (lines 255-257 and 311-312).

> ***Reviewer #2 (Recommendations For The Authors):***
>
> *Several concerns are raised as shown below.*
>
> *Comment 1: In Fig. 2F, it is surprising that ZP3 disappeared in the ovary from mice at the age of 10 months by MIMS analysis, because quite a few oocytes with intact zona pellucida can still be obtained from mice at this age. Notably, ZP would not be renewed once formed.*

Response 1: To clarify, Figure 2F shows LC-MS/MS data and not MIMS data. As mentioned in the Discussion, the detection of long-lived pools of ZP3 at 6 months cannot be derived from newly synthesized zona pellucidae in growing follicles because they would not have been present during the pulse period. The only way we could detect ZP3 at 6 months is if it forms a primitive zona scaffold in the primordial follicle or if ZPs from atretic follicles of the first couple of waves of folliculogenesis incorporate into the extracellular matrix of the ovary. The lack of persistence of ZP3 at 10 months could be due to protein degradation. Should ZP3 indeed form a primitive zona, its loss at 10 months would be predicted to result in poor formation of a bona fide zona pellucida upon follicle growth. Interestingly, aging has been associated with alterations in zona pellucida structure and function. These data open novel hypotheses regarding the zona pellucida (e.g. a primitive zona scaffold and part of the extracellular matrix) and will require significant further investigation to test. These points are highlighted in the Discussion lines 227-245.

> *Comment 2: To determine whether those proteins that can not be identified by MIMS at the time point of 10 months are degraded or renewed, the authors should randomly select some of them to examine their protein expression levels in the ovary by immunoblotting analysis.*

Response 2: To clarify, proteins were identified by LC-MS/MS and not MIMS which was used to visualize long lived macromolecules. Each protein will be comprised of old pools (15N containing) and newly synthesized pools (14N containing). Degradation of the old pool of protein does not mean that there will be a loss of total protein. Moreover, immunoblotting cannot distinguish old and newly synthesized pools of protein. Where overall peptide counts are listed for each protein identified at both time points. As peptides derive from proteins, the table provided with the manuscript reflects what immunoblotting would, but on a larger and more precise scale.

> *Comment 3: I think those proteins that can be identified by MIMS at the time point of 6 months but not 10 months deserve more analyses as they might be the key molecules that drive ovarian aging.*

Response 3: This comment conflicts with comment 2 from Reviewer #3 (Recommendations For The Authors). This underscores that different researchers will prioritize the value and follow up of such rich datasets differently. We agree that the LLP identified at 6 months are of particular interest to reproductive aging, and we are planning to follow up on these in future studies.

> *Comment 4: Figure 1 – figure supplement 1 C-F, compared with the published literature, the numbers of follicles at different developmental stages and ovulated oocytes at both ages of 6 months and 10 months were dramatically low in this study. For 6-month-old female mice, the reproductive aging just begins, thus these numbers should not be expected to decrease too much. In addition, follicle counting was carried out only in an area of a single section, which is an inaccurate way, because the numbers and types of follicles in various sections differ greatly. Also, the data from a single section could not represent the changes in total follicle counts.*

Response 4: We have addressed these points in response to Comment 1 in the Reviewer #2 Public Review, and corresponding changes in the text have been noted.

> *Comment 5: The study lacks follow-up verification experiments to validate their MIMS data.*

Response 5: Two independent mass spectrometry approaches (MIMS and LC-MS/MS) were used to validate the presence of long-lived macromolecules in the ovary and oocyte. Studies focused on the role of specific long-lived proteins in oocyte and ovarian biology as well as how they change with age in terms of function, turnover, and modification are beyond the scope of the current study but ongoing. We have acknowledged these important next steps in the manuscript text (lines 286-288 and 311-312).

> ***Reviewer #3 (Recommendations For The Authors):***
>
> *Comment 1: The authors used the 6-month mice group to represent the aged model, and examined the LLPs from 1 month to 6 months. Indeed, 6-month-old mice start to show age-related changes; however, for the reproductive aging model, the most widely accepted model is that 10-month-old age mice start to show reproductive-related changes and 12-month-old mice (corresponding to 35-40 year-old women) exhibit the representative reproductive aging phenotypes. Therefore, the data may not present the typical situation of LLPs during reproductive aging.*

Response 1: As described in the response to Comment 1 in the Reviewer #3 Public Review, there were clear logistical and technical feasibility reasons why the 6 month and 10-month timepoints were selected for this study. Importantly, however, these timepoints do represent a reproductive aging continuum as evidenced by age-related changes in multiple parameters. Furthermore, there were ultimately very few LLPs that remained at 10 months in both the oocyte and ovary, so inclusion of the 6-month time point was an important intermediate. Whether the LLPs at the 6-month timepoint serve as a protective mechanism in maintaining gamete quality or whether they contribute to decreased quality associated with reproductive aging is an intriguing dichotomy which will require further investigation. This has been added to the discussion (lines 247-257).

> *Comment 2: Following the point above, the authors examined the ovaries in 6 months and 10 months mice by proteomics, and found that 6 months LLPs were not identical compared with 10 months, while there were Tubb5, Tubb4a/b, Tubb2a/b, Hist2h2 were both expressed at these two time points (Fig 2B), why the authors did not explore these proteins since they expressed from 1 month to 10 months, which are more interesting.*

Response 2: The objective of this study was to profile the long-lived proteome in the ovary and oocyte as a resource for the field rather than delving into specific LLPs at a mechanistic level. That being said, we wholeheartedly agree with the reviewer that the proteins that were identified at both 6 month and 10 months are the most robust and long lived and worthy of prioritizing for further study. Interestingly, Tubb5 and Tubb4a have high homology to primate-specific Tubb8, and Tubb8 mutations in women are associated with meiosis I arrest in oocytes and infertility (Dong et al., 2023; Feng et al., 2016). Thus, perturbation of these specific proteins by virtue of their long-lived nature may be associated with impaired function and poor reproductive outcomes. We have highlighted the importance of these LLPs which are present at both timepoints and persist to at least 10 months in the manuscript text (lines 259-270).

> *Comment 3: The authors also need to provide a hypothesis or explanation as to why LLDs from 6 months LLPs were not identical compared with 10 months.*

Response 3: We agree that LLDs identified at 10 months should be also identified as long-lived at 6 months. This is a common limitation of mass spectrometry-based proteomics where each sample is prepared and run individually, which introduces variability between biological replicates, especially when it comes to low abundant proteins. It is key to note that just because we do not identify a protein, it does not mean the protein is not there – it merely means that we were not able to detect it in this particular experiment, but low levels of the protein may still be there. To compensate for this known and inherent variability, we have applied stringent filtering criteria where we required long-lived peptides to be identified in an independent MS scan (alternative is to identify peptide in either heavy or light scan and use modeling to infer FA value based on m/z shift), which gave us peptides of highest confidence. Ideally, these experiments would be done using TMT (tandem mass tag) approach. However, TMT-based experiments typically require substantial amount of input (80-100ug per sample) which unfortunately is not feasible with oocytes obtained from a limited number of pulse-chased animals. We have added this explanation to the discussion (lines 265-270).

> *Comment 4: The reviewer thinks that LLPs from 6 months to 10 months may more closely represent the long-lived proteins during reproductive aging.*

Response 4: We fully agree that understanding the identity of LLPs between the 6 month and 10 month period will be quite informative given that this is a dynamic period when many of LLPs get degraded and thus might be key to the observed decline in reproductive aging. This is a very important point that we hope to explore in future follow-up studies.

> *Comment 5: The authors used proteomics for the detection of ovaries and oocytes, however, there are no validation experiments at all. Since proteomics is mainly for screening and prediction, the authors should examine at least some typical proteins to confirm the validity of proteomics. For example, the authors specifically emphasized the finding of ZP3, a protein that is critical for fertilization.*

Response 5: Thank you, we agree that closer examination of proteins relevant and critical for fertilization is of importance. However, a detailed analysis of specific proteins fell outside of

the scope of this study which aimed at unbiased identification of long-lived macromolecules in ovaries and oocytes. We hope to continue this important work in near future.

> *Comment 6: For the oocytes, the authors indicated that cytoskeleton, mitochondria-related proteins were the main LLPs, however, previous studies reported the changes of the expression of many cytoskeleton and mitochondria-related proteins during oocyte aging. How do the authors explain this contrary finding?*

Response 6: Our findings are not contrary to the studies reporting changes in protein expression levels during oocyte aging – the two concepts are not mutually exclusive. The average FA value at 6-month chase for oocyte proteins is 41.3 %, which means that while 41.3% of long-lived proteins pool persisted for 6 months, the other 58.7% has in fact been renewed. With the exception of few mitochondrial proteins (Cmkt2 and Apt5l), and myosins (Myl2 and Myh7), which had FA values close to 100% (no turnover), most of the LLPs had a portion of protein pools that were indeed turned over. Moreover, we included new data analysis illustrating that we identify comparable number of mitochondrial proteins between the two time points, indicating that while the long-lived pools are changing over time, the total content remains stable (Figure 3 – figure supplement 1E-G).

> *Comment 7: The authors also should provide in-depth discussion about the findings of the current study for long-lived proteins. In this study, the authors reported the relationship between these "long-lived" proteins with aging, a process with multiple "changes". Do long-lived proteins (which are related to the cytoskeleton and mitochondria) contribute to the aging defects of reproduction? or protect against aging?*

Response 7: This is a very important comment and one that needs further exploration. The fact is – we do not know at this moment whether these proteins are protective or deleterious, and such a statement would be speculative at this stage of research into LLPs in ovaries and oocytes. Future work is needed to address this question in detail.

Briley, S. M., Jasti, S., McCracken, J. M., Hornick, J. E., Fegley, B., Pritchard, M. T., & Duncan, F. E. (2016). Reproductive age-associated fibrosis in the stroma of the mammalian ovary. *Reproduction*, *152*(3), 245-260. https://doi.org/10.1530/REP-16-0129

Chiang, T., Duncan, F. E., Schindler, K., Schultz, R. M., & Lampson, M. A. (2010). Evidence that Weakened Centromere Cohesion Is a Leading Cause of Age-Related Aneuploidy in Oocytes. *Current Biology*, *20*(17), 1522-1528. https://doi.org/10.1016/j.cub.2010.06.069

Dong, J., Jin, L., Bao, S., Chen, B., Zeng, Y., Luo, Y., Du, X., Sang, Q., Wu, T., & Wang, L. (2023). Ectopic expression of human TUBB8 leads to increased aneuploidy in mouse oocytes. *Cell Discov*, *9*(1), 105. https://doi.org/10.1038/s41421-023-00599-z

Duncan, F. E., Jasti, S., Paulson, A., Kelsh, J. M., Fegley, B., & Gerton, J. L. (2017). Age-associated dysregulation of protein metabolism in the mammalian oocyte. *Aging Cell*, *16*(6), 1381-1393. https://doi.org/10.1111/acel.12676

Feng, R., Sang, Q., Kuang, Y., Sun, X., Yan, Z., Zhang, S., Shi, J., Tian, G., Luchniak, A., Fukuda, Y., Li, B., Yu, M., Chen, J., Xu, Y., Guo, L., Qu, R., Wang, X., Sun, Z., Liu, M., . . . Wang, L. (2016). Mutations in TUBB8 and Human Oocyte Meiotic Arrest. *N Engl J Med*, *374*(3), 223-232. https://doi.org/10.1056/NEJMoa1510791

Fornasiero, E. F., & Savas, J. N. (2023). Determining and interpreting protein lifetimes in mammalian tissues. *Trends Biochem Sci*, *48*(2), 106-118. https://doi.org/10.1016/j.tibs.2022.08.011

Hark, T. J., & Savas, J. N. (2021). Using stable isotope labeling to advance our understanding of Alzheimer's disease etiology and pathology. *J Neurochem*, *159*(2), 318-329. https://doi.org/10.1111/jnc.15298

Kerr, J. B., Hutt, K. J., Michalak, E. M., Cook, M., Vandenberg, C. J., Liew, S. H., Bouillet, P., Mills, A., Scott, C. L., Findlay, J. K., & Strasser, A. (2012). DNA damage-induced primordial follicle oocyte apoptosis and loss of fertility require TAp63-mediated induction of Puma and Noxa. *Mol Cell*, *48*(3), 343-352. https://doi.org/10.1016/j.molcel.2012.08.017

Kimler, B. F., Briley, S. M., Johnson, B. W., Armstrong, A. G., Jasti, S., & Duncan, F. E. (2018). Radiation-induced ovarian follicle loss occurs without overt stromal changes. *Reproduction*, *155*(6), 553-562. https://doi.org/10.1530/REP-18-0089

Kirkland, J. L. (2013). Translating advances from the basic biology of aging into clinical application. *Exp Gerontol*, *48*(1), 1-5. https://doi.org/10.1016/j.exger.2012.11.014

Mara, J. N., Zhou, L. T., Larmore, M., Johnson, B., Ayiku, R., Amargant, F., Pritchard, M. T., & Duncan, F. E. (2020). Ovulation and ovarian wound healing are impaired with advanced reproductive age. *Aging (Albany NY)*, *12*(10), 9686-9713. https://doi.org/10.18632/aging.103237

Perrone, R., Ashok Kumaar, P. V., Haky, L., Hahn, C., Riley, R., Balough, J., Zaza, G., Soygur, B., Hung, K., Prado, L., Kasler, H. G., Tiwari, R., Matsui, H., Hormazabal, G. V., Heckenbach, I., Scheibye-Knudsen, M., Duncan, F. E., & Verdin, E. (2023). CD38 regulates ovarian function and fecundity via NAD(+) metabolism. *iScience*, *26*(10), 107949. https://doi.org/10.1016/j.isci.2023.107949

Quan, N., Harris, L. R., Halder, R., Trinidad, C. V., Johnson, B. W., Horton, S., Kimler, B. F., Pritchard, M. T., & Duncan, F. E. (2020). Differential sensitivity of inbred mouse strains to ovarian damage in response to low-dose total body irradiationdagger. *Biol Reprod*, *102*(1), 133-144. https://doi.org/10.1093/biolre/ioz164

Savas, J. N., Toyama, B. H., Xu, T., Yates, J. R., 3rd, & Hetzer, M. W. (2012). Extremely long-lived nuclear pore proteins in the rat brain. *Science*, *335*(6071), 942. https://doi.org/10.1126/science.1217421

Toyama, B. H., Savas, J. N., Park, S. K., Harris, M. S., Ingolia, N. T., Yates, J. R., 3rd, & Hetzer, M. W. (2013). Identification of long-lived proteins reveals exceptional stability of essential cellular structures. *Cell*, *154*(5), 971-982. https://doi.org/10.1016/j.cell.2013.07.037

https://doi.org/10.7554/eLife.93172.2.sa0